3B2v8.06a/w (Dec 5 2003).51c XML:ver:5.0.1 CSR : 1215 Prod.Type:FTP pp.1–38(col.fig.:1–8,10,11,16–18,20,21,23) ED:MangalaK. PAGN:Uday SCAN:Global

ARTICLE IN PRESS

Available online at www.sciencedirect.com

SCIENCE DIRECT®

ELSEVIER

Continental Shelf Research ▮ (▮▮▮▮) ▮▮▮–▮▮▮

CONTINENTAL SHELF RESEARCH

www.elsevier.com/locate/csr

A cross-scale model for 3D baroclinic circulation in estuary–plume–shelf systems: II. Application to the Columbia River

António M. Baptista[a,*], Yinglong Zhang[a], Arun Chawla[a], Mike Zulauf[a], Charles Seaton[a], Edward P. Myers III[a,b], John Kindle[c], Michael Wilkin[a], Michela Burla[a], Paul J. Turner[a]

[a] *OGI School of Science and Engineering, Oregon Health and Science University, 20000 NW Walker Road, Beaverton, OR 97006, USA*

[b] *National Ocean Service, National Oceanic and Atmospheric Administration, Office of Coastal Survey, Silver Spring, MD 20910-3282, USA*

[c] *Ocean Sciences Branch, Naval Research Laboratory, Stennis Space Center, MS 39529, USA*

Abstract

This article is the second of a two-part paper on ELCIRC, an Eulerian-Lagrangian finite difference/finite volume model designed to simulate 3D baroclinic circulation across river-to-ocean scales. In part one (Zhang et al., 2004), we described the formulation of ELCIRC and assessed its baseline numerical skill. Here, we describe the application of ELCIRC within CORIE, a coastal margin observatory for the Columbia River estuary and plume. We first introduce the CORIE modeling system and its multiple modes of simulation, external forcings, observational controls, and automated products. We then focus on the evaluation of highly resolved, year-long ELCIRC simulations, using two variables (water level and salinity) to illustrate simulation quality and sensitivity to modeling choices. We show that, process-wise, simulations capture well important aspects of the response of estuarine and plume circulation to ocean, river, and atmospheric forcings. Quantitatively, water levels are robustly represented, while salinity intrusion and plume dynamics remain challenging. Our analysis highlights the benefits of conducting model evaluations over large time windows (months to years), to avoid significant localized biases. The robustness and computational efficiency of ELCIRC has proved invaluable in identifying and reducing non-algorithmic sources of errors, including parameterization (e.g., turbulence closure and stresses at the air-water interface) and external forcings (e.g., ocean conditions and atmospheric forcings).

Keywords: Mathematical modeling; Ocean, coastal, and estuarine circulation; Eulerian–Lagrangian methods; Finite volumes; Finite differences; Semi-implicit methods.

*Corresponding author. Tel.: 1 503 748 1147; fax: 1 503 748 1273.
E-mail address: baptista@ccalmr.ogi.edu (A.M. Baptista).

0278-4343/$ - see front matter © 2005 Published by Elsevier Ltd.
doi:10.1016/j.csr.2004.12.003

1. Introduction

Integrated observatories (Clark and Isern, 2003; Martin, 2003; USCOP, 2004) are expected to dramatically improve the understanding of the ocean across scales and processes, and to provide unprecedented, objective information to address societal priorities regarding ocean preservation and utilization. Meeting these lofty expectations will require improvements in underlying technologies (e.g., models, platforms, sensors, and information technologies), as well as adjustments in their use.

A preview of challenges to come has been provided by selected prototype ocean observatories (Parker, 1997; Glenn et al., 2000; Steere et al., 2000; Rhodes et al., 2001; Baptista, 2002). Developed and maintained since 1996 for the Columbia River estuary and plume, CORIE (CCALMR, 1996–2004; Baptista et al., 1998; Baptista et al., 1999) is one such prototype. CORIE was designed from the onset as a multi-purpose, regional infrastructure for research, education, and management. The design includes three integrated components: a real-time observation network, a modeling system, and a web-based information system.

Perhaps surprisingly, of the three CORIE components, the modeling system has posed the most fundamental challenges, calling for new modeling technologies and paradigms. In particular, we found the need to develop a new cross-scale 3D baroclinic circulation code (ELCIRC; Zhang et al., 2004) in order to meet operational requirements of efficiency and quality. Also, automated integrative procedures—including the generation of model forcings, quality controls and modeling products—have become essential to creating, improving, and interpreting simulations. Moreover, multiple simulation modes—including daily forecasts, multi-year hindcasts, and scenario simulations—forced the development of multi-scale, long-term calibration and validation strategies and procedures.

Here, we describe the CORIE modeling system (Section 2) and present selected results (Section 3), with emphasis on water levels and salinities. The description of the modeling system is intended as a reference for derivative papers, which will complement the present work by exploring in further depth specific modeling aspects, and scientific and management applications of CORIE. The results in Section 3 illustrate the extent to which the modeling system is already able to describe complex, multi-scale circulation processes in the Columbia River and help identify directions for further improvement. In Section 4, we discuss implications for derivative research on Columbia River circulation, for further algorithmic development of cross-scale numerical models and for coastal estuarine and plume modeling within the requirements of ocean observatories.

2. The CORIE modeling system

One of the world's classic river-dominated estuaries, the Columbia River, is a highly dynamic system that responds dramatically to changes in ocean tides and water properties, regulated river discharges, and coastal winds. A dominant hydrographic feature on the U.S. west coast, the Columbia River plume exports dissolved and particulate matter hundreds of kilometers along and across the continental shelf (Barnes et al., 1972; Grimes and Kingsford, 1996). In response to seasonal changes of the largescale coastal circulation patterns, the plume typically develops northward along the coastal shelf in fall and winter, and southwestward offshore of the shelf in spring and summer. However, the direction, thickness, and width of the plume—and, in particular, the near-field plume—can change in hours to days in response to local winds (CCALMR, 1996–2004; Hickey et al., 1998; Garcia-Berdeal et al., 2002).

Compressed and often stratified, the Columbia River estuary is subject to extreme variations in salinity intrusion and stratification regime (Hamilton, 1990; Jay and Smith, 1990; Chawla et al., in prep.). Two main channels (one dredged for navigation) cut the otherwise shallow estuary (Fig. 1). A shallow coastal region north of the Columbia River mouth combines with Coriolis to establish an underlying tendency for the near-plume to move north. This northward tendency is countered

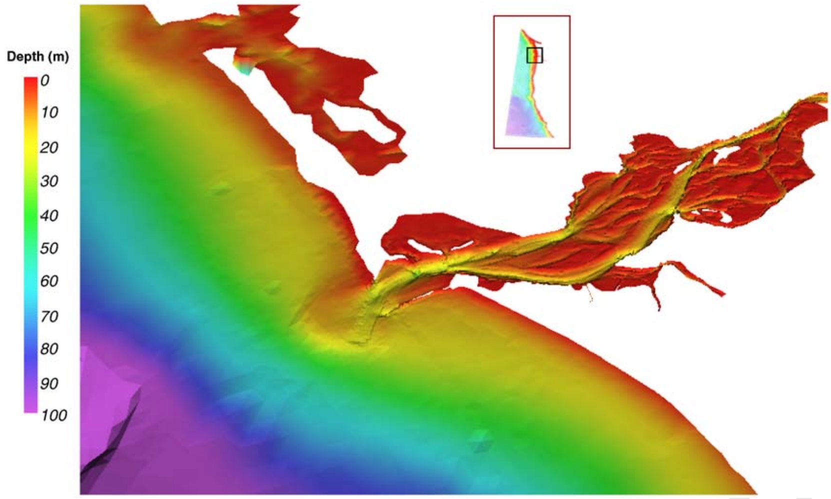

Fig. 1. The North Channel and Navigation Channel cut the otherwise shallow Columbia River estuary. Lateral bays are shallow and ecologically important environments. Shallow bathymetry immediately North of the mouth of the estuary combines with Coriolis to naturally bend the plume northward in the absence of winds.

by the exit angle of the navigation channel and is either countered or reinforced by local winds.

The CORIE modeling system integrates *models*, *forcings*, and *quality controls* to produce daily forecasts and multi-year simulation databases of circulation in both the estuary and the plume (Fig. 2). Data assimilation is used only sparingly (Section 2.3). Elements of complexity for the simulations include: (a) highly variable and non-linear forcings (e.g., wind, tides, river discharge); (b) dynamic density fronts and strong buoyancy-driven flow; and (c) broad range of inter-connected spatial (from under 100 m to well above 10 km) and temporal scales (minutes to decades).

To address these complexities, we found it necessary to develop a new 3D baroclinic circulation model, ELCIRC. The motivation, formulation, and basic skill assessment of ELCIRC have been presented in Zhang et al. (2004). In summary, ELCIRC is a finite-difference/finite-volume model, based on unstructured grids; the numerical scheme is robust, volume conservative, and computationally efficient. Within the constraints of the hydrostatic approximation, the ELCIRC physical formulation allows for a unified river-to-ocean approach, allying to features of state-of-the-art coastal ocean models the ability to treat estuary features such as regions of high advection and of extensive wetting and drying.

Taking advantage of the characteristics of ELCIRC, the domain of simulation spans from the Bonneville Dam and the Willamette Falls, approximately 240 km upstream of the entrance to the Columbia River estuary, to and beyond the continental shelf of California, Oregon, Washington, and British Columbia. Included in the domain, albeit at low resolution, are the straits of Juan de Fuca and Georgia, and the Puget Sound. Computational grids (Fig. 3; see also Figs. 6a and 15c for local details) are typically 3D, unstructured in the horizontal plane, with z-coordinates in the vertical. Computational and archival requirements are met with a dedicated computer infrastructure. At the time of this writing, the infrastructure includes 20 dual CPU Intel compute nodes (2.4 GHz, 4 Gb) organized as a Beowulf cluster and 28 TB of online disk arrays. For a baroclinic simulation on a typical computational grid (34190 horizontal nodes; 50622 horizontal hybrid elements; 62 z-levels) and with a typical time step (1.5 minutes), ELCIRC runs 2.5–3 times faster than real time in a single CPU. The upper bound in this range applies to simulations with a zero-equation turbulence closure, and

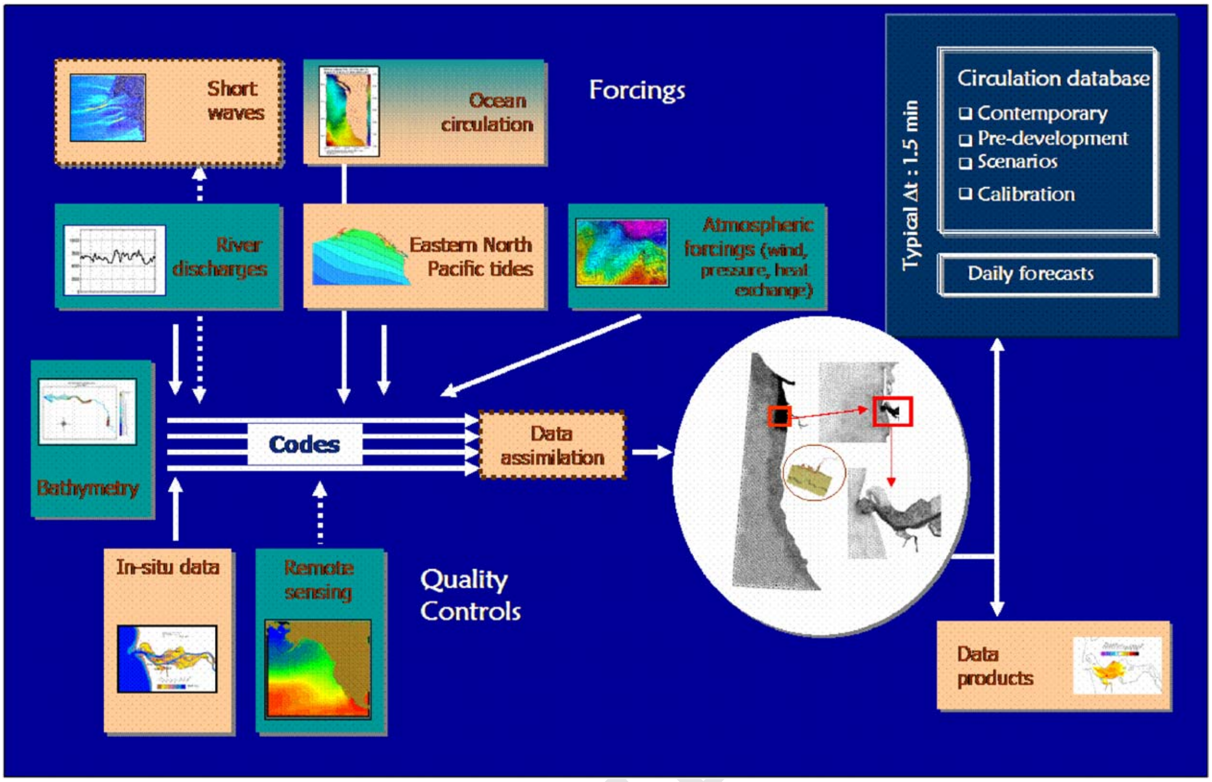

Fig. 2. The CORIE modeling system integrates models with external forcings, quality controls, and products.

the lower bound applies to simulations with a 2.5-equation turbulence closure. Purely barotropic simulations can be run with a 15-min time step and are about 60 times faster than real-time. However, rarely is it justified to run a barotropic simulation in the Columbia River, due to strong buoyancy effects. About 0.8 TB of online storage is required to store a typical year-long baroclinic simulation.

2.1. External forcings

Ocean, atmospheric, and river influences control much of the dynamics of the Columbia River estuary and plume. All of these influences are highly variable in space and time. It is essential to account for this variability, for a successful simulation of circulation. We describe below strategies and information sources to characterize external forcings in the CORIE modeling system. Where they diverge, we briefly note differences between strategies to address forcings for daily forecasts and strategies for retrospective simulations (hindcast databases and calibration runs).

2.1.1. River inputs

The Columbia River and the Fraser River watersheds are the dominant freshwater source for the Pacific Northwest (see Fig. 3 for geographic reference), and both are accounted for in the CORIE modeling system. Within the Columbia River, freshwater inputs are considered from the Bonneville Dam (for the main stem of the Columbia River) and from Newberg (for the Willamette River). Neglected are smaller freshwater inputs, including those from the Cowlitz, Lewis, and Sandy rivers. Bonneville discharges retain—despite heavy hydropower regulation—substantial seasonal (e.g., spring freshets) and inter-annual variability (e.g., in response to El

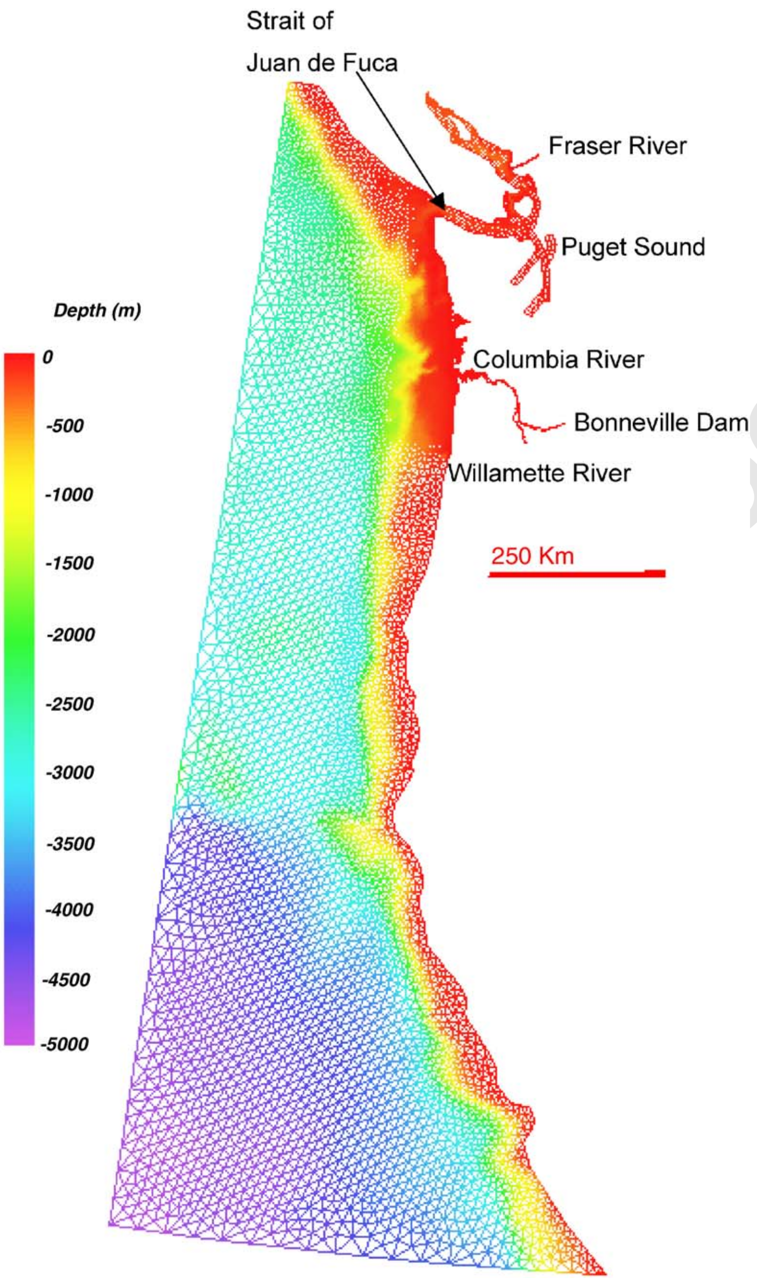

Fig. 3. The computational domain extends from California, through Oregon and Washington, to British Columbia. Grids are hybrid and resolution is finest in the estuary and near plume (e.g., see details in Figs. 6a and 15c).

Niño—Southern Oscillation and in response to Pacific—Decadal Oscillation).

For retrospective simulations, information on freshwater discharge is obtained from two USGS (US Geological Survey) gauges: USGS-ID 14128870, downstream of the Bonneville dam; and USGS-ID 14197900, at Newberg. Temperature data for Columbia River are obtained from the same site that records the river discharge. Temperature data for Willamette River are obtained from a USGS gauge in Portland (USGS-ID 14211720), located about 60 km downstream of the Newberg gauge. Data from the same gauges are used for the daily forecasts through short-term extrapolation. Fraser discharge is taken from the Hope gauge (08MF005) of Environment Canada. For forecasts, the actual discharge values are unavailable, so they are replaced with a discharge climatology based on 1912–2003 data. Fraser temperature is extracted from the NCOM model results (see below).

2.1.2. Ocean conditions

We have used four semi-diurnal (M_2, S_2, N_2, K_2) and four diurnal (K_1, O_1, P_1, Q_1) constituents to characterize ocean tides at the boundaries of the CORIE computational domain. Spatially variable tidal amplitudes and phases are available for the Eastern North Pacific from at Egbert et al. (1994) and Myers and Baptista (2001). We typically use Myers and Baptista (2001) (e.g., Table 1) after early tests showed limited sensitivity to the choice of one or another source. Nodal factors and astronomical arguments are calculated from the tidal package of Foreman (1977). No low-frequency set-up was imposed at the boundaries. The earth tidal potential (from Reid, 1990) can be included but is typically neglected.

Seasonal climatology for ocean salinity and temperature is available from Levitus (1982). However, Levitus climatology is notably coarse in particular for coastal applications and is inherently unable to capture the inter-annual variability of salinity and temperature. As an alternative to climatology, we use the output from operational Navy products to define ocean salinity and temperature conditions, using 2002 hindcast database simulations as the benchmark. Developed by the Naval Research Laboratory for application to coastal and global prediction of ocean dynamic and thermodynamic fields (Martin, 2000), the Navy Coastal Ocean Model (NCOM) is a variant of the Princeton Ocean Model (POM; Blumberg and Mellor, 1987). NCOM runs using 1/8th degree horizontal resolution and 40 vertical levels that are a combination of sigma levels in the upper 150 m of the ocean and *z*-levels from 150 m to the ocean bottom (Rhodes et al., 2001). This model has been tested using both climatological forcings and real time atmospheric forcings from the Navy's Operational Global Atmospheric Prediction System (NOGAPS; Rosmond et al., 2002). Global NCOM has been spun up from a climatological state to the present, using a combination of NOGAPS forcings and the assimilation of satellite altimeter data and 3D temperature and salinity observations derived from the Modular Ocean Data Assimilation System (MODAS; Fox et al., 2002). By default, we use NCOM results to define the initial oceanic salinity and temperature (S, T) conditions as well as for nudging ELCIRC S, T results in the ocean (Section 2.3).

To date, CORIE simulations have relied on the internal physics of the ELCIRC model and on external (winds and atmospheric pressure) and internal (density gradients) forcings to generate ocean set-up and circulation within the modeling domain.

2.1.3. Atmospheric forcings

Several different atmospheric forcings are utilized by the CORIE modeling system. They are divided into two main groups: near-surface atmospheric properties and downwelling radiative fluxes at the surface. The atmospheric properties include the *x*- and *y*-components of the wind at a height of 10 m, the surface atmospheric pressure (reduced to mean sea level), the air temperature at 2 m, and the specific humidity at 2 m. The radiative fluxes include the downwelling shortwave (solar) and the downwelling longwave (infrared) radiations at the water surface.

These forcing data have been compiled from a number of different sources, but the data fall into two broad divisions: locally archived forecast data and re-analysis data (essentially hindcast simulations with extensive data assimilation of available observations). The forecast datasets include data from: (a) the National Oceanic and Atmospheric Administration (NOAA) National Centers for Environmental Prediction (NCEP) Global Forecast System (GFS, also referred to as the MRF and/or AVN forecasts); (b) NCEP Eta Model; and

(c) the Advanced Regional Prediction System developed at the University of Oklahoma, as modified and run at Oregon State University (OSU/ARPS). The reanalysis dataset originates from a joint project of NCEP and the National Center for Atmospheric Research (NCAR; the NCAR/NCEP Global Reanalysis Project).

2.2. Observational controls

Inherent to the concept of the CORIE modeling system are systematic quality controls based on comparisons of data from various long-term observational networks (Figs. 4 and 5). Most of these networks have real-time or quasi real-time telemetry, thus supporting both hindcast simulations (databases and calibration runs) and daily forecasts.

The CORIE real-time observation network covers the estuary extensively and the near-ocean sparingly (Fig. 4; CCALMR (1996–2004)). At each station, in situ sensors measure various combinations of water temperature, salinity, pressure, velocity, and atmospheric parameters. Observations are available in both real-time and long-term archives, some extending nearly 8 years. We have also equipped the M/V Forerunner, a 50-foot vessel, with a pump-through, conductivity–temperature sensor and a hull-mounted acoustic Doppler profiler. The vessel is also used for targeted CORIE cruises (e.g., Fig. 20).

Other observation networks used include NOAA Center for Operational Oceanographic Products and Services (CO-OPS), NOAA National Data Buoy Center (NDBC), U.S. Army Corps of Engineers (USACE), and USGS (cf. Fig.

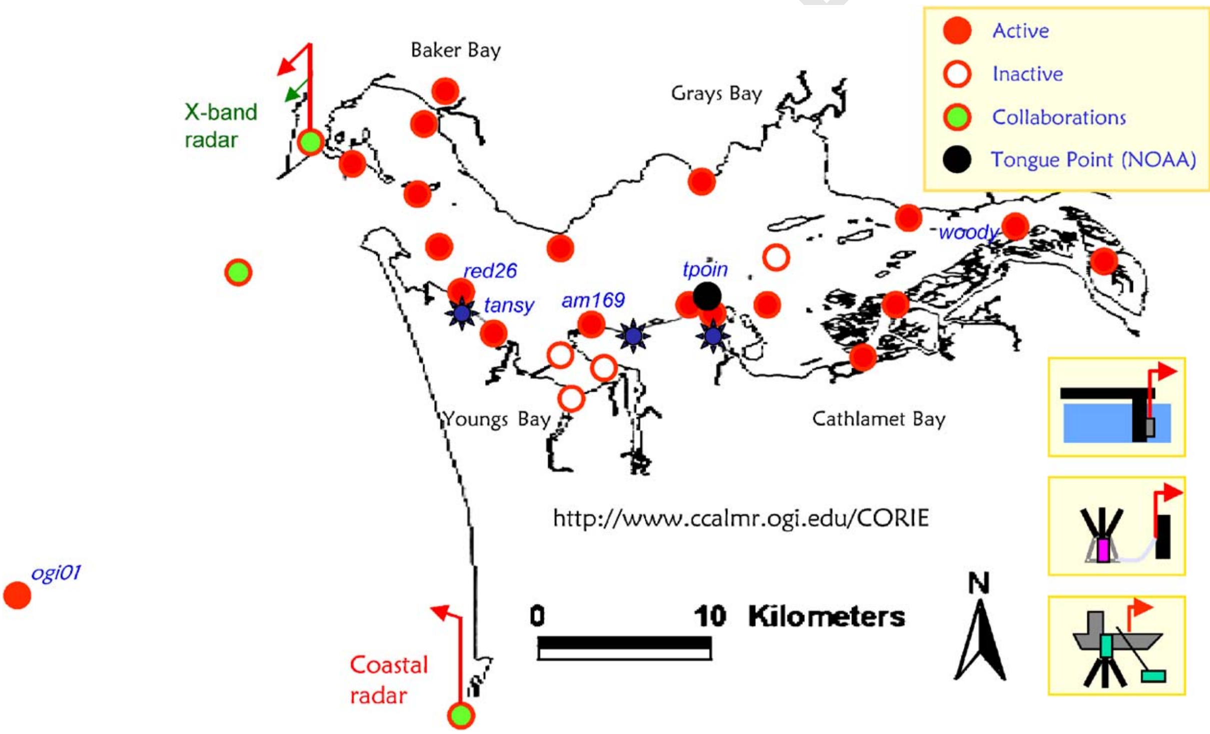

Fig. 4. Fixed stations of the CORIE observation network are concentrated on the estuary up to the limit of salinity intrusion, with an offshore presence through station *ogi*01. Most stations are in piles or similar structures, but Acoustic Doppler profilers (available at five stations: *ogi*01, *red*26, *tansy*, *am*169, and *am*012) require either bottom (in the estuary) or surface (shelf) frames or buoys. Besides fixed stations, CORIE includes a mobile station in the form of a training vessel. The configuration of the CORIE network and its sensors is still evolving; see (CCALMR, 1996–2004) for a current configuration. The planned deployment of a short range high-frequency radar and an x-band radar is through collaborations with researchers Oregon State University.

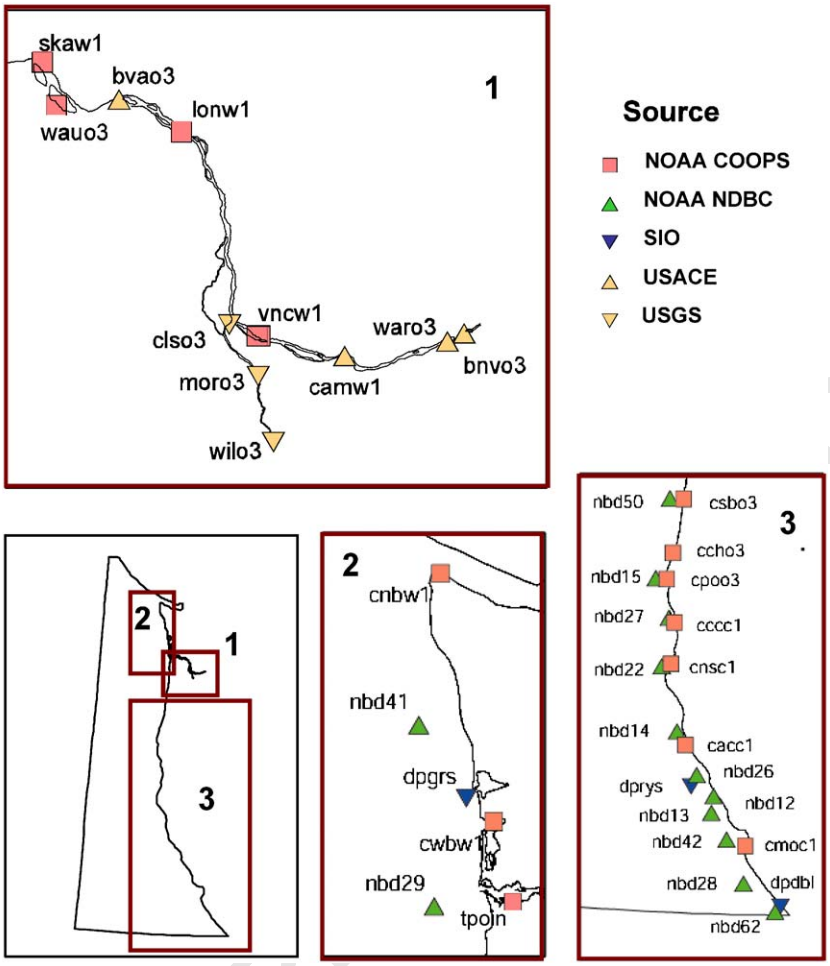

Fig. 5. Other observation networks in the region. NOAA COOPS stations provide tidal elevation data, NDBC buoys provide atmospheric winds and pressure information, and USGS and USACE gauges provide river discharge and/or temperature information.

5). Besides systematic quality control of CORIE simulations against information from long-term fixed observation networks, the CORIE modeling system also conducts more "random" quality controls against episodic data from a variety of sources. Particularly useful are Synthetic Aperture Radar satellite images (e.g., Fig. 15a) and diverse oceanographic cruises.

Key oceanographic cruises include: (a) an extensive 1990–1991 plume study with moorings and vessels (Hickey et al., 1998); (b) extensive estuarine cruises in the Columbia River estuary conducted as a part of the Columbia River component (CRETM, 1990–2000) of a national land-margin ecosystem research program (LMER Coordinating Committee, 1992); (c) periodic CORIE cruises in the Columbia River estuary and plume (since 1996); and (d) cruises conducted by NOAA Fisheries since 1998 along coastal transects in California, Oregon, and Washington, and at or near the mouth of the Columbia River. Recently, extensive Columbia River plume surveys were conducted in May–July of 2004, by two different but overlapping multi-investigator teams, using diverse and sophisticated observation techniques from land, airborne, and in-water (moored and mobile) platforms (Section 3.1).

2.3. Data assimilation and nudging

The CORIE philosophy is that the numerical circulation model is ultimately responsible for representing the physics inside the domain, once appropriate choices have been made for parameters and external forcings. Thus, the CORIE modeling system has used data assimilation sparingly: primarily, for improving the definition of external forcings and for off-line optimization of empirical parameters.

Specifically, data assimilation was used to define ocean tidal forcings (Myers and Baptista, 2001) and is being used to optimize bottom friction (Frolov et al., 2004). In addition, under certain circumstances, ocean conditions (S, T) are locally nudged to information from either global circulation models or climatology—which in turn, have been either data-assimilated or objectively analyzed from data. With this nudging, we seek to impose non-reflective ocean boundary conditions and to moderate errors in heat-balance calculations resulting from specifying imprecise atmospheric forcings.

Nudging is accomplished through a simple algorithm:

$$\widehat{\beta^n}(x,y,z) = (1-\alpha)\beta^n_{ELCIRC}(x,y,z) + \alpha\beta^n_{base}(x,y,z) \qquad (1)$$

with

$$\alpha(x,y,z) = \gamma(x,y)\psi(z),$$

where $\widehat{\beta^n}$ is the nudged value at time n, β^n_{ELCIRC} is the value computed directly by solving the governing equations, and β^n_{base} is the reference value from a global circulation model or from climatology. The nudging factor γ is typically zero in the estuary and near-plume but increases toward the ocean in patterns dictated by the objectives of the particular simulation. The vertical nudging profile ψ is linear or piece-wise linear.

2.4. Products

The large number of simulations conducted daily within CORIE requires systematic, standardized processing. Automated procedures have been established for separate but similar processing of daily forecasts and of hindcast simulations (both hindcast databases and calibration runs). The results of hindcast simulations are publicly accessible (CCALMR, 1996–2004).

3. Selected results

Simulations of Columbia River circulation are sensitive—often in complex, nonlinear manners—to a wide range of modeling choices, including initialization strategies and representation of internal parameters, bathymetry, and external forcings.

To understand and to address this sensitivity, we have developed a sustained, iterative strategy that involves simulations at multiple time windows. Anchoring this process are hindcast circulation databases that extend for one or more years and that take 2–3 months to generate. Databases reflect best-available modeling choices at the beginning of their generation, and those choices are kept unchanged throughout the generation of the entire database.

Complementary calibration runs are, however, also used in parallel to advance the state-of-the-art in CORIE simulations. Thus, it is rare that a database is completed without one or more modeling choices being shown to be non-optimal—and this information feeds the next database. The duration of calibration runs is typically between one week and several months.

As an illustration of our strategy, in Section 3.1 we will describe a baseline simulation and will then summarize how alternative modeling options affect the representation of processes and variables. We will focus our analysis on just two variables: water levels and salinity. Velocities and temperatures will be addressed in separate publications. However, because salt propagation is essentially a transport problem, the present analysis already provides a stringent, albeit indirect, assessment of the circulation capabilities of the numerical model.

3.1. Baseline simulation

We take as a reference a specific circulation database 11 (DB11) and focus on its results for 2002. At the time of this writing, DB11 is the most current and comprehensive CORIE database, covering 1999-present. As typical in CORIE, DB11 modeling choices incorporate lessons learned in several previous databases and calibration runs (e.g., Section 3.2). Shortcomings detected during the generation of DB11 have already inspired parallel calibrations runs (e.g., Section 3.2). Table 5 summarizes parameters used in DB11, as well as in other databases and calibration runs presented in this paper.

3.1.1. Simulation set-up

DB11 was constructed by combining multiple simulation ensembles conducted in parallel. Each ensemble is composed of about 3 months, run sequentially. To minimize discontinuities across ensembles, contiguous ensembles overlap by two (or more if needed) weeks: the first two weeks of each ensemble are considered warm-up and are eventually discarded in favor of the last weeks of the previous ensemble. The rationale behind this "temporal" parallelization hinges on the hypothesis that a dynamic equilibrium is established within each ensemble. This hypothesis will be tested below. All simulations include nudging of ocean S, T to NCOM results, which also provide initial conditions for each simulation ensemble.

The computational grid uses a combination of quadrangles and triangles, with highest spatial resolution concentrated in the Columbia River estuary and near plume. Over 35% of the elements in the grid have an equivalent diameter between 100 and 200 m (Fig. 6). Upstream of the estuary, the main river channel is carefully delineated, but flood plains are often under-detailed. Thus, that part of the grid functions primarily to delineate a conduit for freshwater discharge into the estuary, with expectations of local accuracy low.

Horizontal resolution and local geometric detail are driven by two concerns: minimizing deviations from grid orthogonality, a constraint imposed by the ELCIRC algorithm (Zhang et al., 2004); and keeping numerical diffusion under control. As discussed in detail elsewhere (Baptista et al., 2004), we have already achieved orthogonality for most elements in the grid (Fig. 7b,d), but further grid refinement is useful to reduce numerical diffusion (Fig. 11), and thus to enhance the ability of ELCIRC to represent coastal eddies and other sharp spatial features.

The vertical grid consists of 62 z-levels, with finer resolution concentrated on the top 30 meters of the water column (Fig. 8). As typical in z-coordinate models, near-bottom representation is challenging for ELCIRC. With our choice of vertical and horizontal grids, difficulties in the estuary and near plume are minimized, at the expense of the continental shelf, continental slope, and deep ocean (Fig. 9).

Capitalizing on the ability of ELCIRC to handle Courant numbers well above unity, a time step of 1.5 min is used. With this time step, Courant numbers as large as 4 (in the estuary; Fig. 10) and even 10 (upriver; figure not shown) are common. A time step of as large as 15 min would still have been appropriate for purely barotropic simulations. However, time steps larger than 1.5 min lead to parasitic oscillations in the vicinity of strong baroclinic forcings.

To understand these oscillations, we note that a Courant–Friedrich–Lévy condition associated with the baroclinic term can be estimated via the maximum internal wave speed as

$$C'_u = \frac{\Delta t \sqrt{g'h}}{\Delta x} \leqslant 1, \quad (2)$$

where $g' = g\Delta\rho/\rho_0$ is the reduced gravity. Therefore, a theoretical maximum time step for stability can be estimated as

$$\Delta t_{\max} \sim \frac{175}{\sqrt{9.8 * 25/1025 * 20}} \cong 79\,\mathrm{s}, \quad (3)$$

assuming a typical channel depth of $h = 20$ m, a horizontal resolution of 175 m (e.g., see Fig. 6), and an extreme case of freshwater ($\rho = 1000\,\mathrm{kg/m^3}$) at the surface and saltwater ($\rho = 1025\,\mathrm{kg/m^3}$) at the bottom. This order-of-magnitude estimate lends credence to the trial and error

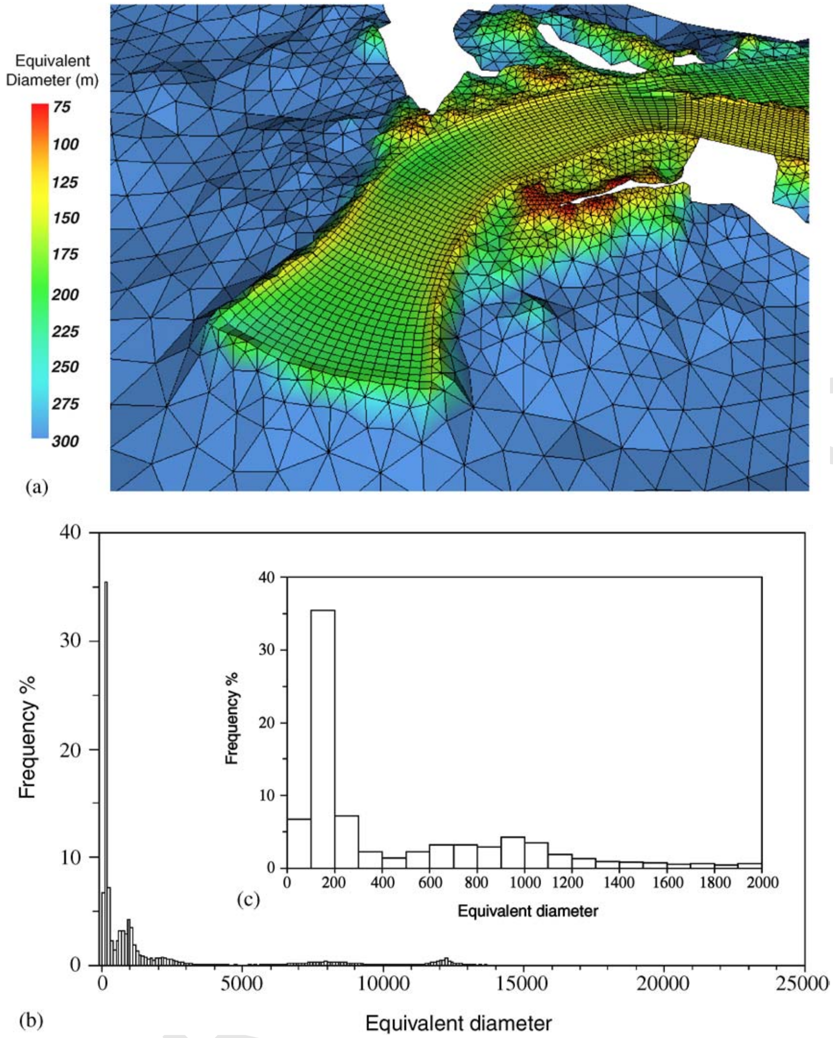

Fig. 6. Equivalent diameters near the Columbia River entrance for a typical CORIE grid. (a) Isolines; both color and "relief" indicate the magnitude of the equivalent diameter. (b) Histogram. (c) A zoom into the histogram for equivalent diameters up to and including 2000 m.

analysis that led to the choice of an operational time step of 1.5 min.

Based on the formal analysis of Casulli and Cattani (1994), we set the implicitness factor θ (see Eq. (37) in Zhang and Baptista, 2004) to 0.6 for best accuracy, thus weighing the present time step slightly more than the previous time step in treating terms of the continuity and momentum equations that are handled implicitly. Empirical trial-and-error supported this choice.

By default, in ELCIRC, the tracking of characteristic lines is performed with a simple Euler integration. N integration steps (referred to as sub-time steps) are allowed for tracking between times $n+1$ and n. In DB11, we let the sub-time step be chosen automatically, to account for local gradients of velocity. Specifically:

$$N = \max\{N_{min}, \min[N_{max}, \max(N_x, N_y, N_z)]\} \quad (4)$$

where N_{min} and N_{max} are user-specified limits (2

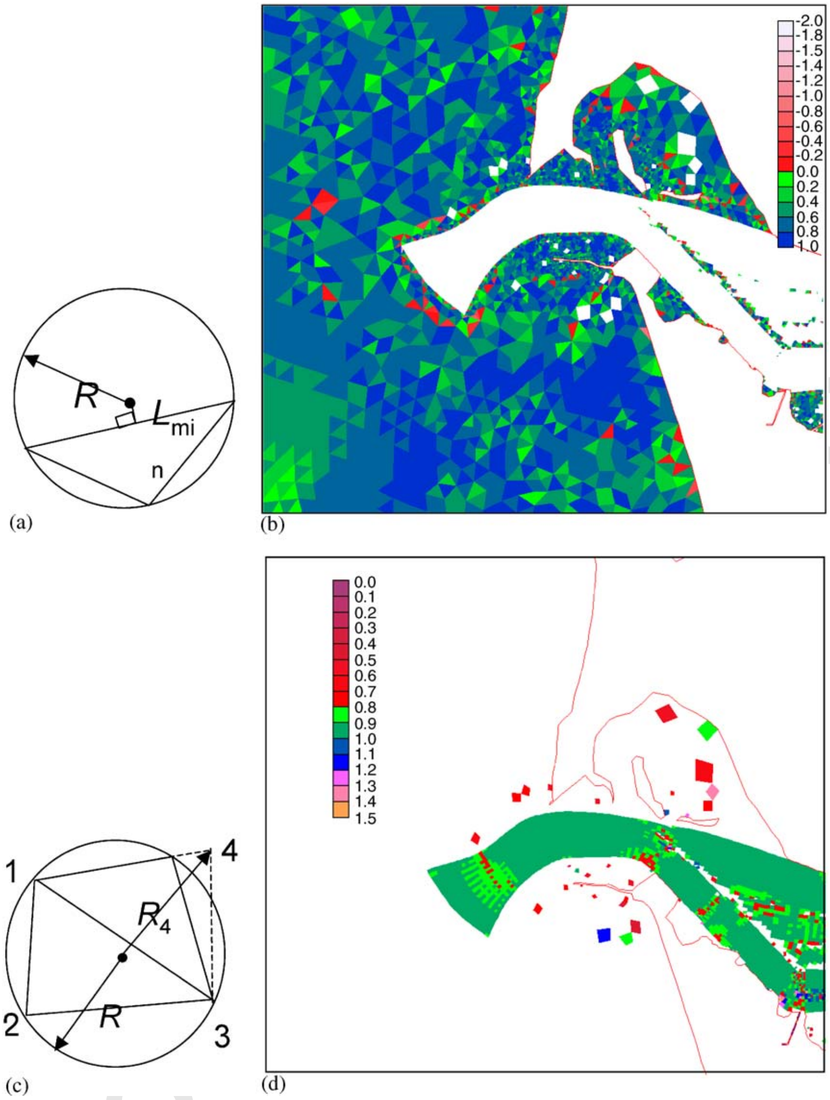

Fig. 7. Orthogonality indices θ. (a) and (c): Definition sketches for a triangle and quadrangle. (b) and (d): Indices for triangles and quadrangles. For orthogonal triangles, $\theta > 0$. For orthogonal quadrangles, $\theta = 1$.

and 9, for DB11) and

$$N_x = 10\left|\frac{\partial u}{\partial l}\right|\Delta t, \quad N_y = 10\left|\frac{\partial v}{\partial l}\right|\Delta t, \quad N_z = \frac{|w|\Delta t}{\Delta z}, \tag{5}$$

where u, v, and w are velocities in the x, y, and z directions; horizontal gradients $|\partial u/\partial l|$ and $|\partial v/\partial l|$ are computed along sides of elements; and Δz is the local vertical grid size. Experiments where we enforced smaller sub-time steps or tracked the characteristic lines using higher-order methods (e.g., 5th order Runge–Kutta) revealed no substantial gains in accuracy (results not shown).

Three types of physical parameterization play potentially important roles in the model output: bottom friction, surface stress, and vertical mixing. Choices for DB11 were as follows:

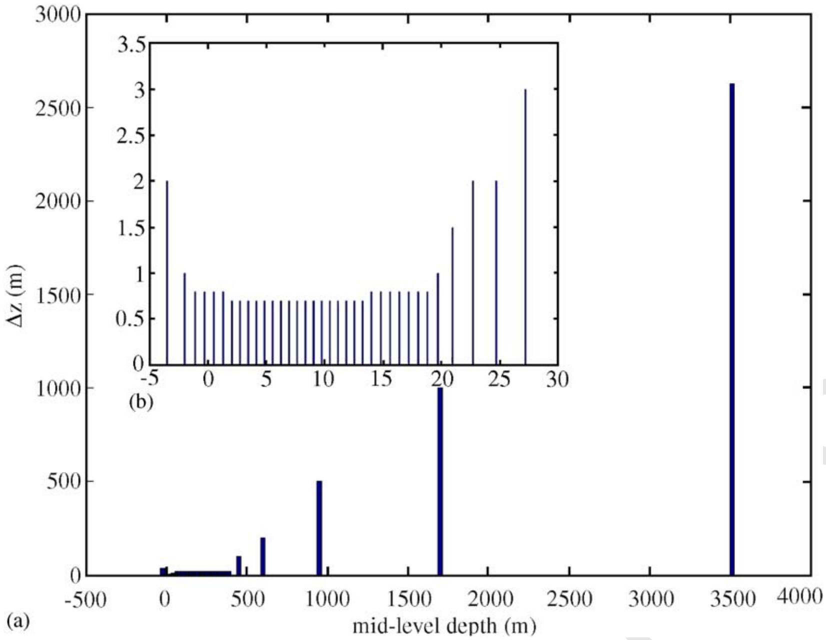

Fig. 8. Vertical discreatization, as represented by Δz, is shown as a function of depth (a), including a detail inset for the top 30 m (b).

Bottom friction: The existence of different bed forms in the Columbia River, upstream and downstream of the Astoria–Tongue Point region, has long been recognized (Hamilton, 1990). We coarsely represent this difference by imposing a spatially varying bottom drag coefficient (C_{Db}; see Eq. (14) in Zhang et al., 2004). Specifically, we allow for a frictionless bottom ($C_{Db} = 0$) in the continental shelf and in the Columbia River up to 20 km upstream of the estuary entrance, we impose substantial friction ($C_{Db} = 0.0045$) above 30 km upstream of the estuary entrance, and we let C_{Db} transition linearly between these two regions. While characterization of bottom friction is not a closed issue for the Columbia River (e.g., Frolov et al., 2004), improvements of model results based on optimizing values of C_{Db} have been modest. Internal calculations of C_{Db} based on matching model velocities with bottom boundary layer profiles (Eq. (15) in Zhang et al., 2004) have not proved clearly superior, either, possibly because of the difficulty of z-coordinate models such as ELCIRC in representing the bottom boundary layer (Fig. 11).

Surface stress: Through sensitivity analysis, partially reported in Section 3.2, we found that the bulk aerodynamic algorithm of Zeng et al. (1998) to be superior to more traditional, simpler, but less process-driven surface stress formulations (e.g., see review in Pond and Pickard, 1998). As described in Zhang et al. (2004), the algorithm of Zeng et al. (1998) accounts for surface layer stability, free convection, and variable roughness length at the ocean-atmosphere interface. This algorithm is now standard in the CORIE modeling system whenever simulations (such as in DB11) use the output of atmospheric models to drive wind fields and heat balance budgets.

Vertical mixing: ELCIRC offers various alternatives to characterize vertical mixing (see Section 2.4 of Zhang et al., 2004). DB11 uses a k-kl closure, with mixing limits imposed as shown in Table 5. The choice of different mixing limits was meant to reflect different mixing regimes inside and outside the estuary and, more specifically, to prevent over-mixing inside the estuary. The choice has significant implications for the results (see Section 3.2).

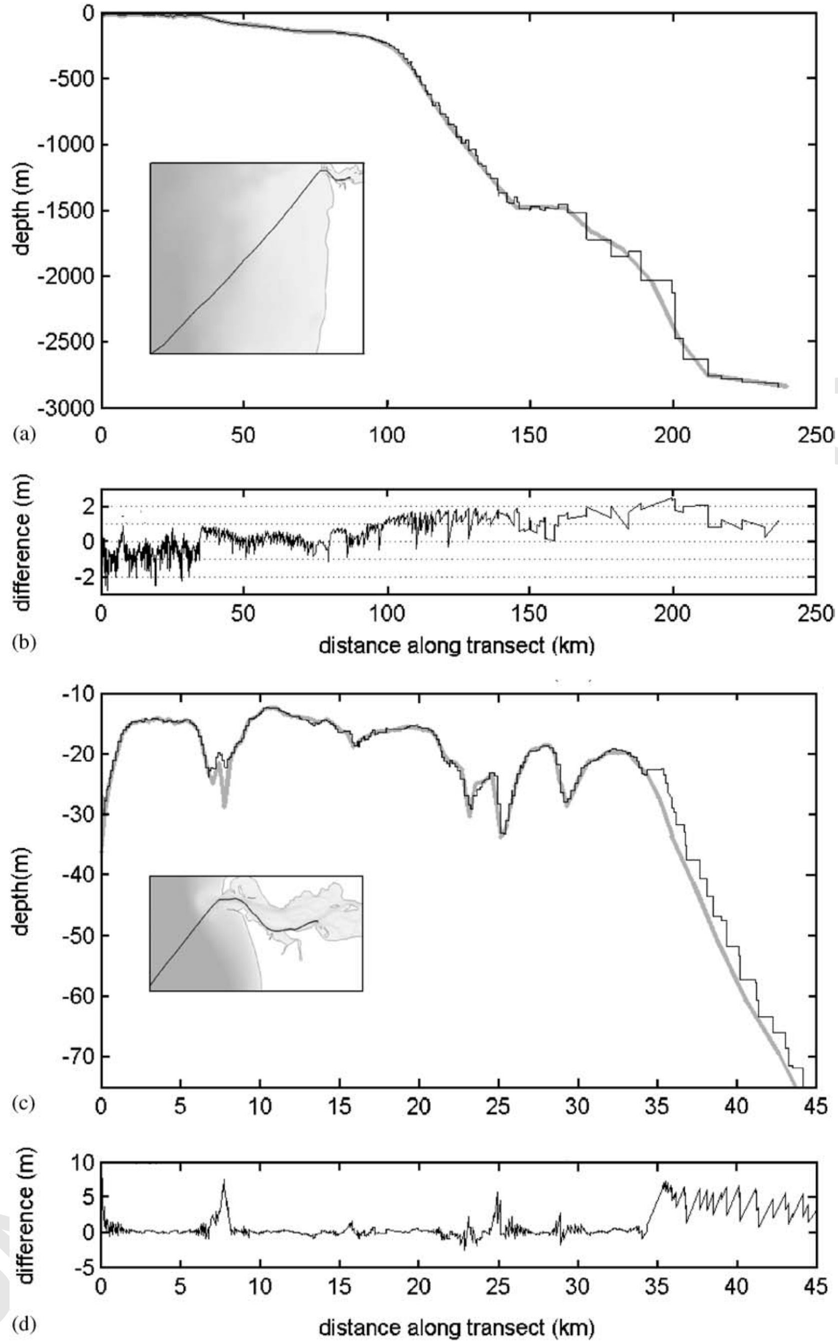

Fig. 9. Bottom representation in the numerical model. (a) The actual bathymetry in 'gray' and its representation in the model in 'black' along a transect extending from the estuary to offshore. The orientation of the transect is shown in the inset map. Distance (km) is from the origin of the transect inside the estuary. (b) The difference between the model representation and actual bathymetry. Positive values indicate regions where the model bathymetry is shallower than actual bathymetry. (c)–(d) The same transect but zoomed inside the estuary.

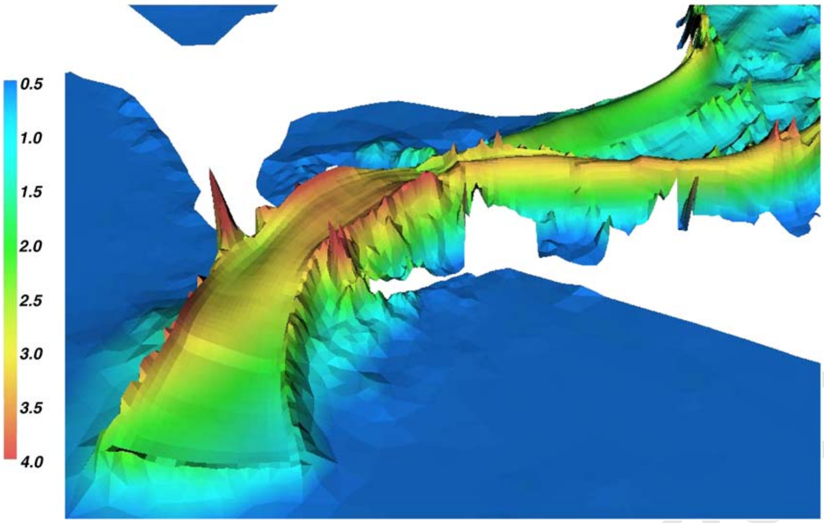

Fig. 10. Estimated Courant number near the Columbia River entrance for a high-discharge condition. Both color and "relief" indicate the magnitude of the Courant number, which approaches 4 in the region shown.

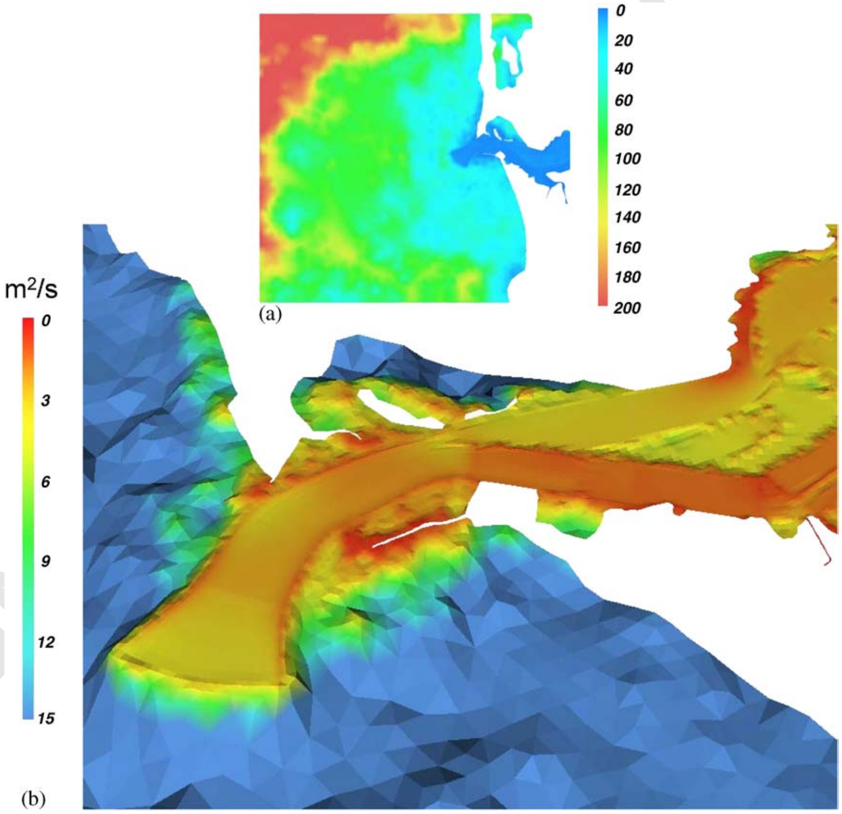

Fig. 11. Maximum numerical diffusivity (m^2/s) near the Columbia River entrance. Both color and "relief" indicate the magnitude of the numerical diffusivity. The 2D inset shows a larger area, generally with larger numerical diffusivity because of lower resolution.

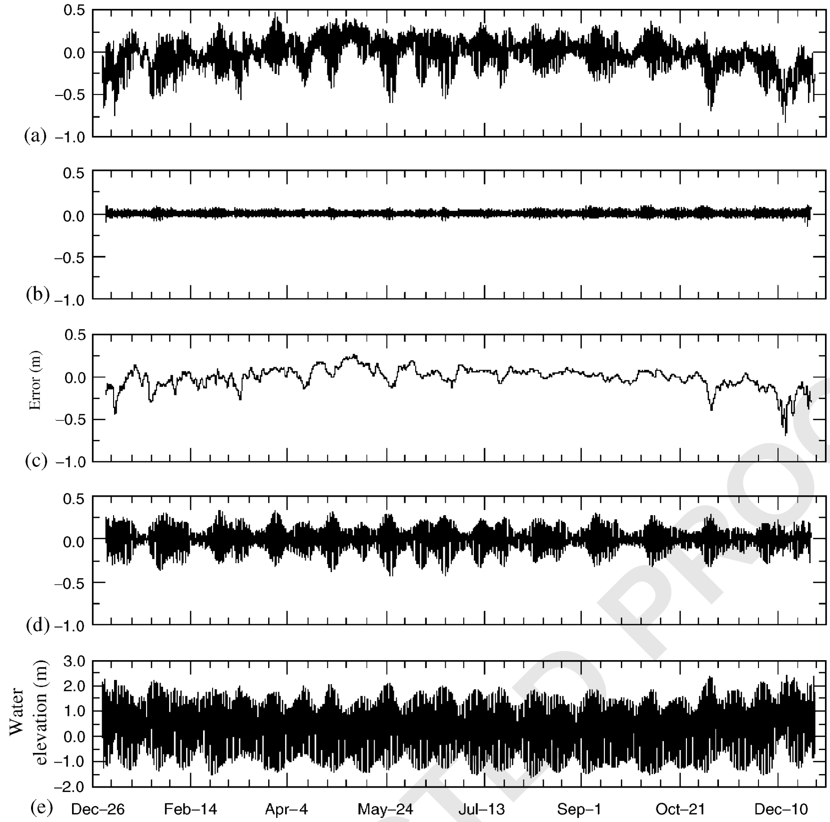

Fig. 12. DB11 simulations of 2002 water levels at Tongue Point. (a) Total error. (b) High-pass error. (c) Low-pass error. (d) Band-pass error. (e) Observed water-level data. Water levels and errors are shown in meters.

Arguably, external forcings, in particular the ocean conditions and atmospheric forcings, are currently the single most significant source of uncertainty for CORIE simulations (see Section 2.1 for the details for initial and boundary conditions). In DB11, S, T approximately 300 km or more from the mouth of the estuary are nudged to NCOM results, with a maximum nudging factor of 5% (see Section 2.3).

3.1.2. Representation of water levels

We first consider water levels at a single station, Tongue Point (or *tpoin*, using the CORIE 5-digit terminology for field stations). A station of the NOAA CO-OPS tidal network (Fig. 5), Tongue Point is located inside the estuary, about 30 km upstream from the entrance (Fig. 4). Long-term water-level observations, with accurate vertical data, are available; the record for 2002, in particular, is uninterrupted (Fig. 12e).

DB11 provides a robust description of Tongue Point water levels. The average error[1] for a full-year simulation is −0.01 m, with a standard deviation of 0.188 m and a root mean square error of 0.188 m. Water levels are over-estimated at most by 0.658 m and are underestimated at most by 0.848 m. Histograms of errors are shown in Fig. 13, both for the full signal and for specific frequency bands, defined as *low pass* ($T > 30$ h), *band pass* ($9.6\,\text{h} \leqslant T \leqslant 30\,\text{h}$; i.e., in the astronomic tidal range), and *high pass* ($T < 9.6$ h; i.e., inclusive of shallow water tides).

[1]Throughout this paper, model error is defined as "simulations minus observations". This definition ignores observation errors, but is sufficient for the purposes of our discussion.

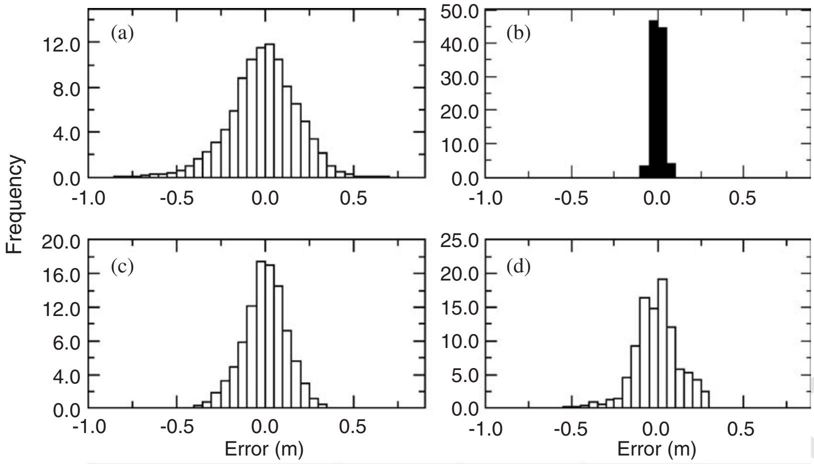

	(a)	(b)	(c)	(d)
RMS error	0.19	0.03	0.12	0.14
Average error	-0.01	0.00	0.00	-0.01
Error standerd deviatiov	0.19	0.03	0.12	0.14
95 percentile (over prediction)	0.28	0.05	0.20	0.22
95 percentile (under prediction)	-0.34	-0.05	-0.22	-0.23
Maximum over prediction	0.66	0.13	0.38	0.30
Maximum under prediction	-0.85	-0.14	-0.52	-0.75

Fig. 13. DB11 error statistics for water levels at Tongue Point (in meters) for baseline simulation. (a) Full signal. (b) High-pass. (c) Band-pass. (d) Low-pass.

Time series of errors at Tongue Point (Fig. 12 b, d) suggest that band-pass and high-pass errors respond directly to tidal forcing and tend to be largest during spring tides. Band-pass errors are substantially larger than high-pass errors, reflecting the relative difference of the signals represented (astronomic tides being larger than shallow water tides). While tides are non-stationary in the Columbia River due to interactions with river discharge, harmonic analysis for the full year of 2002 (Tables 1 and 2) provides a useful, if simplified, context. We note, in particular that in most constituents, the tidal amplitudes are overestimated and the model simulations lead the data (smaller phase lag). The exception is the M_6 component, where the amplitudes are underpredicted by the model, thus suggesting insufficient bottom friction.

Low-pass errors (Fig. 12c) show a seasonal trend, with the model tending to overestimate observations in summer and to underestimate them in winter. Strong winter storms in January and December introduce the largest errors (see also Section 3.2). We note that the model is able to generate internally a significant part of the low-pass signal, even though that signal is not forced at the domain boundaries. Coastal winds and atmospheric pressure gradients are responsible for this internal generation.

A comparison of error patterns across selected stations of the NOAA CO-OPS tidal network is shown in Fig. 14 (see Fig. 5 for station locations). There is remarkable spatial coherence at all frequencies, with some informative exceptions. In particular:

- The average error at *cnbw*1, a station at the entrance of the Strait of Juan de Fuca, is substantially larger than that of any other station (cf. Table 3). This may be due to the overly simplistic representation of that part of the domain in the CORIE modeling system. The

Table 1
Illustrative tidal constituents at the ocean boundary and in the Columbia River estuary

	Frequency (rad s^{-1})	Amplitude imposed at ocean boundary (m)[a]			Amplitude at Tongue Point[b] (m)	
		Maximum	Minimum	46°15′N	Data	DB06
M_2	1.405189e − 04	1.0064	0.3395	0.8518	0.9255	0.9987
S_2	1.454441e − 04	0.2923	0.0626	0.2379	0.2400	0.2844
N_2	1.378797e − 04	0.2063	0.0815	0.1733	0.1798	0.1963
K_2	1.458423e − 04	0.0791	0.0145	0.0645	0.1030	0.1129
K_1	7.292117e − 05	0.4666	0.3289	0.4247	0.4651	0.5148
O_1	6.759775e − 05	0.2851	0.191	0.2587	0.3063	0.3173
P_1	7.251056e − 05	0.1461	0.1030	0.1317	0.1158	0.1326
Q_1	6.495457e − 05	0.0498	0.0353	0.0455	0.0504	0.0556
M_4	2.810378e − 04	—	—	—	0.0057	0.0096
M_6	4.215567e − 04	—	—	—	0.0109	0.0035

[a]The ocean boundary of the CORIE modeling domain extends from 35°N to 50°N. 46°15′N is the latitude of the Columbia River entrance. Values are extracted from Myers and Baptista (2001).
[b]Tides are non-stationary in the Columbia River because of the strong nonlinear influences of river discharge. Amplitudes shown for Tongue Point, a NOAA tidal station approximately 30 km upstream of the mouth of the Columbia River, are from harmonic analysis for year 2002. DB06 refers to a specific CORIE simulation (see text, Section 3.1).

Table 2
Comparison of observed and simulated tidal constituents at Tongue Point for 2002

	Amplitude at Tongue Point (m)		Phase at Tongue Point (deg)	
	Data	DB11	Data	DB11
M_2	0.9255	0.9930	159.60	155.34
S_2	0.2400	0.2832	293.85	290.27
N_2	0.1798	0.1952	336.53	323.38
K_2	0.1030	0.1141	310.11	307.12
K_1	0.4651	0.5076	267.87	263.34
O_1	0.3063	0.3183	117.13	110.77
P_1	0.1158	0.1316	256.58	249.91
Q_1	0.0504	0.0595	316.51	308.16
M_4	0.0057	0.0163	249.72	279.20
M_6	0.0109	0.0028	173.10	174.03

effect is seen clearly in the low-pass and band-pass errors (Fig. 14a, c) and in the amplitudes of specific tidal constituents (in particular for M2 and M4; Table 4).

- Low-pass errors (Fig. 14a) tend to show near-synchronous spikes (underestimations) during strong winter storms, consistent with the regional development of frontal systems. The southernmost station (*cmoc*1) is the least correlated of all stations. A detailed analysis of the correlation between frontal systems and water-level responses will be presented in a separate article.
- High-pass errors (Fig. 14b) are typically small and smaller than band-pass errors. The two cases (*cwbw*1 and *skaw*1) where substantial high-pass errors occur are in stations located in shallow areas with very poor grid and bathymetric resolution (in Willapa Bay and in a freshwater confluence of the Columbia River, respectively). High-pass errors at these stations are dominated by shallow water tidal frequencies, an indication that local resolution is insufficient to account for strong tidal nonlinearities occurring in these areas.
- Errors at Tongue Point are generally coherent with dominant errors at coastal stations. However, the spring-neap asymmetry of band-pass errors at Tongue Point is larger than at coastal stations (except for (*cnbw*1 and *cwbw*1), which are affected by special circumstances).

3.1.3. Representation of wetting and drying

The Columbia River is subject to extensive wetting and drying. Representation of this process is challenging, but necessary and within the type of capabilities expected of ELCIRC. In Fig. 15, we provide a snapshot, during low-water conditions, of a SAR image that identifies (with some subjectivity) wet and dry areas, and a DB11 simulation displaying equivalent information. For reference, we also include a representation of the DB11 numerical grid, which permits identification of the areas that are kept permanently dry in the modeling domain. The three images (Fig. 15a–c) are consistently geo-referenced, and the SAR and DB11 images are synoptic within 5 min.

The qualitative agreement between the simulations and the SAR image is remarkably good both in the mainstem of the estuary and in the Cathlamet Bay. We found the results very encouraging relative to the ability of ELCIRC to represent wetting and drying processes.

3.1.4. Representation of salinity fields

Columbia River salinity fields vary dramatically in space and time (Jay and Smith, 1990), with major oceanographic and ecological implications. Multi-scale representation of this variability is extremely challenging and is a major goal of the CORIE modeling system. This paper provides only an introduction to challenges and successes towards this goal. We begin by examining year-long time series of salinities at three stations,

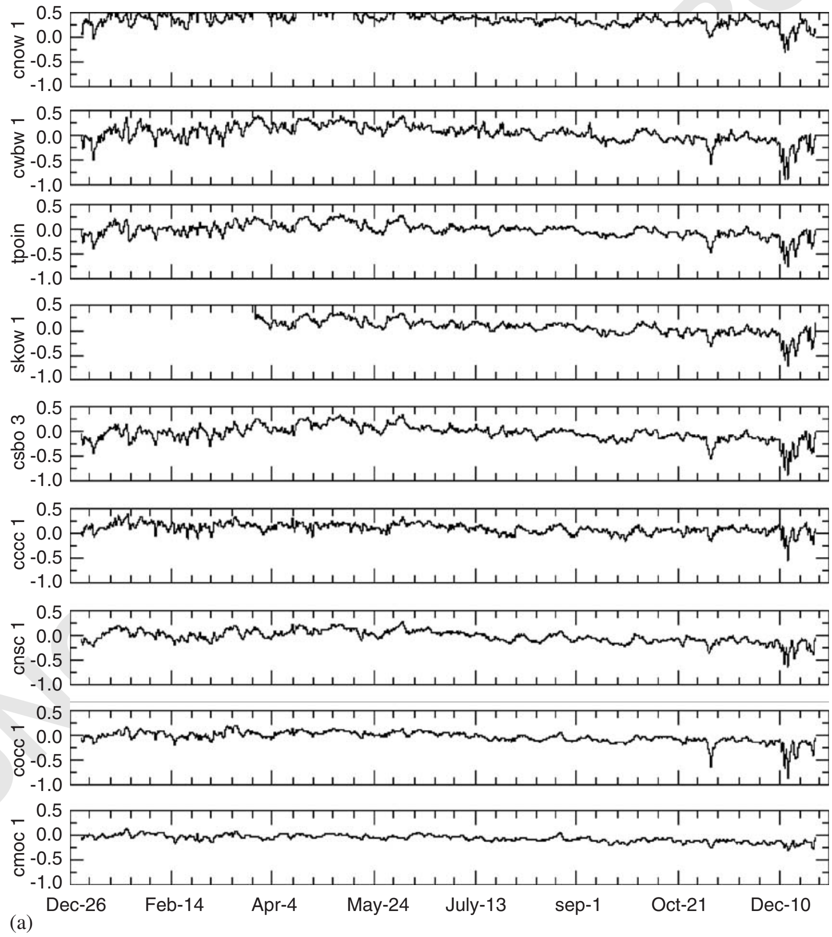

Fig. 14. DB11 errors in water levels at multiple tide gauges along the coast and in the Columbia River system (see Figs. 4 and 5 for locations): (a) Low-pass. (b) High-pass. (c) Band-pass.

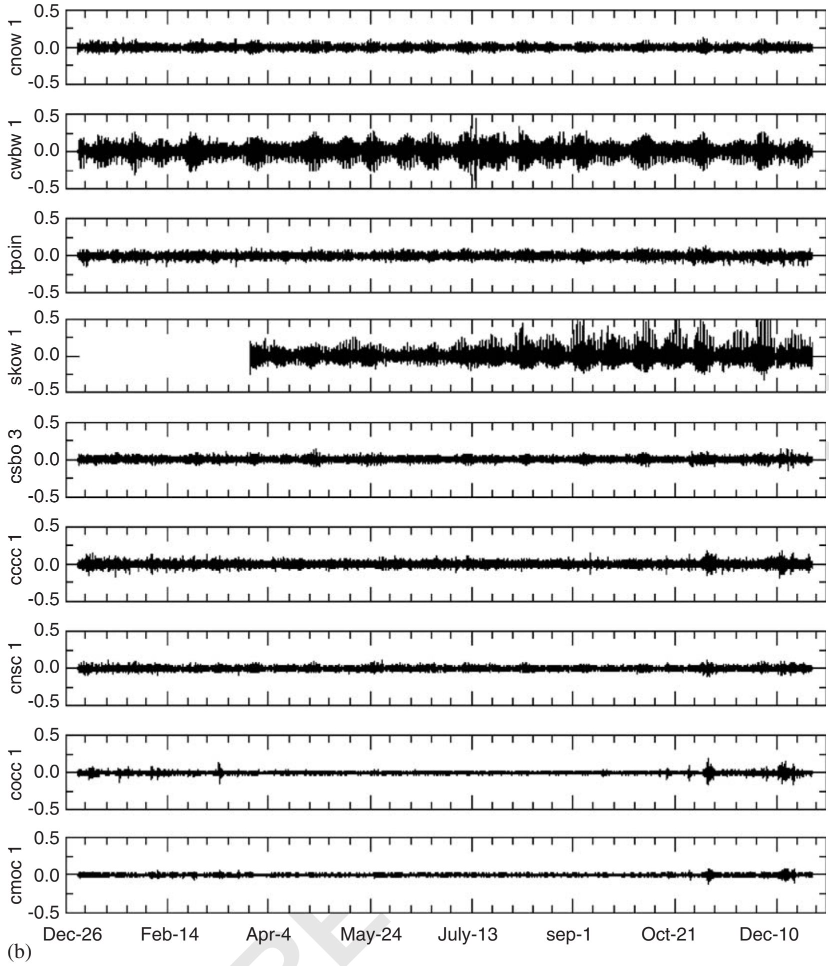

Fig. 14. (*Continued*)

where CORIE sensors are available: *ogi*01, *red*26, and *am*169.

Station *ogi*01 is located in the continental shelf, at a depth of about 100 m, and is approximately 25 km southwest of the mouth of the Columbia River estuary (Fig. 4). The station is in the path of the near plume during periods of northerly wind, which are dominant during the spring and summer. During the winter, southerly winds dominate, and *ogi*01 is off the plume path for extended periods (e.g., see pattern of observed daily maximum and minimum salinities in January and February, Fig. 16a). DB11 simulations (Fig. 16b) show a plume that is responsive to changes in wind direction.

Station *red*26 (Fig. 4) is approximately 13 km upstream of the mouth of the estuary, near the navigation channel. Bottom daily maximum salinities from DB11 track well those salinities observed at the bottom CORIE sensor (Fig. 17). In particular, we note the good correlation between observed and simulated sudden dips in salinity (e.g., at the end of January and beginning of July). The conditions that generate these dips are under investigation, one hypothesis being that the dips coincide with the simultaneous occurrence of downwelling-favorable winds and neap tides.

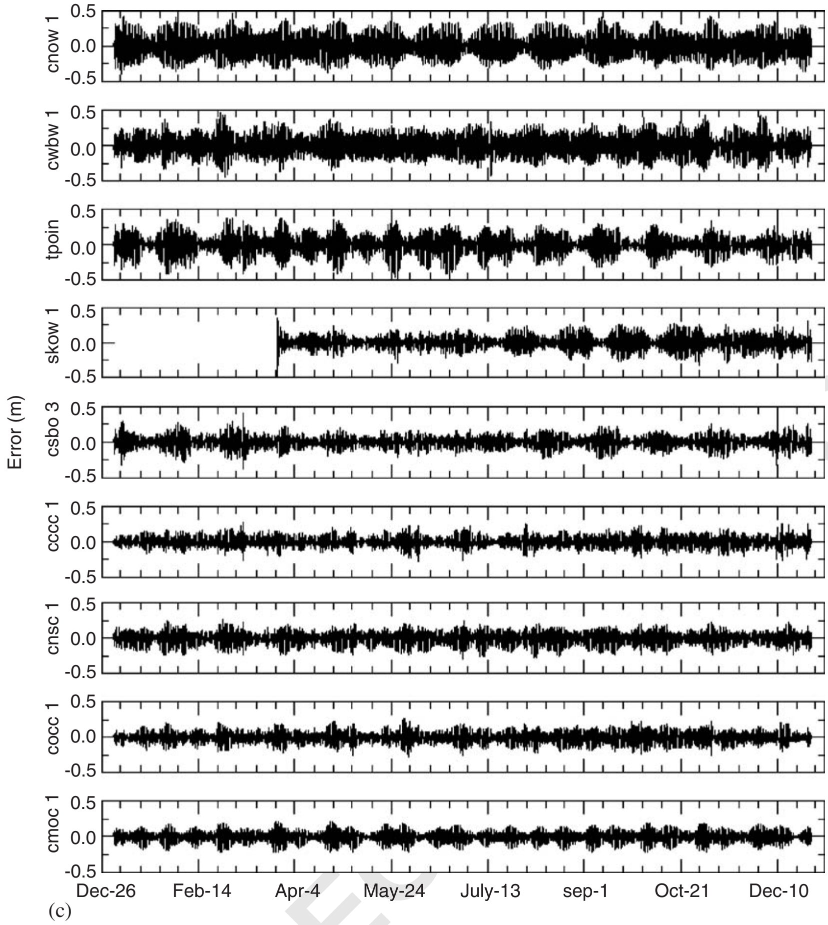

Fig. 14. (*Continued*)

Table 3
Comparison of error statistics for water levels at multiple NOAA CO-OPS for DB11

Stations	Error (m)				
	Average	95% percentiles		Std. Dev.	RMS
*cnbw*1	0.36	0.03	0.67	0.20	0.41
*cwbw*1	0.04	−0.32	0.43	0.23	0.24
tpoin	−0.01	−0.34	0.28	0.19	0.19
*skaw*1	0.07	−0.27	0.34	0.19	0.20
*csbo*3	−0.05	−0.35	0.23	0.18	0.18
*cccc*1	0.10	−0.11	0.30	0.13	0.16
*cnsc*1	−0.03	−0.27	0.21	0.15	0.16
*cacc*1	−0.03	−0.24	0.17	0.14	0.14
*cmoc*1	−0.05	−0.22	0.11	0.10	0.11

Like those observed, daily minimum salinities from DB11 decrease substantially during spring freshets. In general, however, a comparison of observed and simulated salinities, and daily minimum salinities suggests that the simulated estuary is fresher during ebb than it should be, particularly during the latter half of the year.

Station *am*169 (Figs. 4 and 18) is located further upstream in the estuary, approximately 20 km from the mouth and also near the navigation channel. Often fresh during ebb, and occasionally fresh throughout the entire tidal cycle during spans of the spring freshet, *amb*169 is a challenging station to represent numerically. In particular, DB11 shows consistently lower levels of salt than

Table 4
Tidal amplitudes (m) at selected NOAA CO-OPS stations

	*cacc*1		*ccc*1		*ccho*3		*cmoc*1	
	Data	DB06	Data	DB06	Data	DB06	Data	DB06
M_2	0.5686	0.5186	0.7103	0.7003	0.8060	0.7942	0.4890	0.4427
S_2	0.1382	0.1259	0.1825	0.1798	0.2151	0.2114	0.1305	0.1222
N_2	0.1240	0.1082	0.1522	0.1430	0.1696	0.1622	0.1104	0.1028
K_2	0.0419	0.0337	0.0560	0.0508	0.0623	0.0610	0.0409	0.0322
K_1	0.3859	0.4039	0.4068	0.4356	0.4145	0.4526	0.3803	0.3921
O_1	0.2467	0.2338	0.2560	0.2548	0.2591	0.2681	0.2430	0.2234
P_1	0.1167	0.1183	0.1238	0.1275	0.1257	0.1331	0.1157	0.1135
Q_1	0.0438	0.0446	0.0457	0.0489	0.0468	0.0496	0.0432	0.0419
M_4	0.0006	0.0002	0.0007	0.0007	0.0097	0.0003	0.0016	0.0001
M_6	0.0005	0.0001	0.0004	0.0003	0.0040	0.0004	0.0002	0.0001

	*cnbw*1		*cnsc*1		*cpoo*3		*csbo*3	
	Data	DB06	Data	DB06	Data	DB06	Data	DB06
M_2	0.7807	1.0755	0.6815	0.6488	0.7452	0.7492	0.8837	0.8716
S_2	0.2309	0.3125	0.1722	0.1624	0.1963	0.1978	0.2422	0.2401
N_2	0.1672	0.2196	0.1455	0.1338	0.1577	0.1525	0.1870	0.1777
K_2	0.0631	0.0907	0.0497	0.0453	0.0594	0.0578	0.0715	0.0689
K_1	0.5126	0.5028	0.4088	0.4289	0.4432	0.4495	0.4521	0.4662
O_1	0.3210	0.3056	0.2579	0.2504	0.2824	0.2633	0.2798	0.2778
P_1	0.1564	0.1461	0.1247	0.1270	0.1352	0.1270	0.1367	0.1375
Q_1	0.0574	0.0532	0.0456	0.0475	0.0498	0.0504	0.0503	0.0502
M_4	0.0104	0.0013	0.0117	0.0011	0.0008	0.0002	0.0136	0.0010
M_6	0.0073	0.0002	0.0062	0.0007	0.0013	0.0001	0.0072	0.0002

	*cwbw*1	
	Data	DB06
M_2	0.9612	0.8174
S_2	0.2583	0.2249
N_2	0.1970	0.1636
K_2	0.0780	0.0761
K_1	0.4449	0.4481
O_1	0.2749	0.2602
P_1	0.1373	0.1288
Q_1	0.0475	0.0456
M_4	0.0139	0.0465
M_6	0.0083	0.0046

those observed, including a tendency, for most of the year, to predict freshwater conditions during ebb, even at the bottom of the estuary.

The results presented above (and additional results available at CCALMR, 1996–2004) suggest that, on the whole, DB11 salinities are responsive to river forcings, coastal winds, and spring–neap cycles, but that salt penetration in the estuary tends to be under predicted. As a baseline for further analysis in Section 3.2, year-long salt volumes in the estuary (in the form of 15-day running averages) and plume volumes (defined by the 30psu contour) are plotted in Fig. 19 against the river discharge at Bonneville Dam. The salt

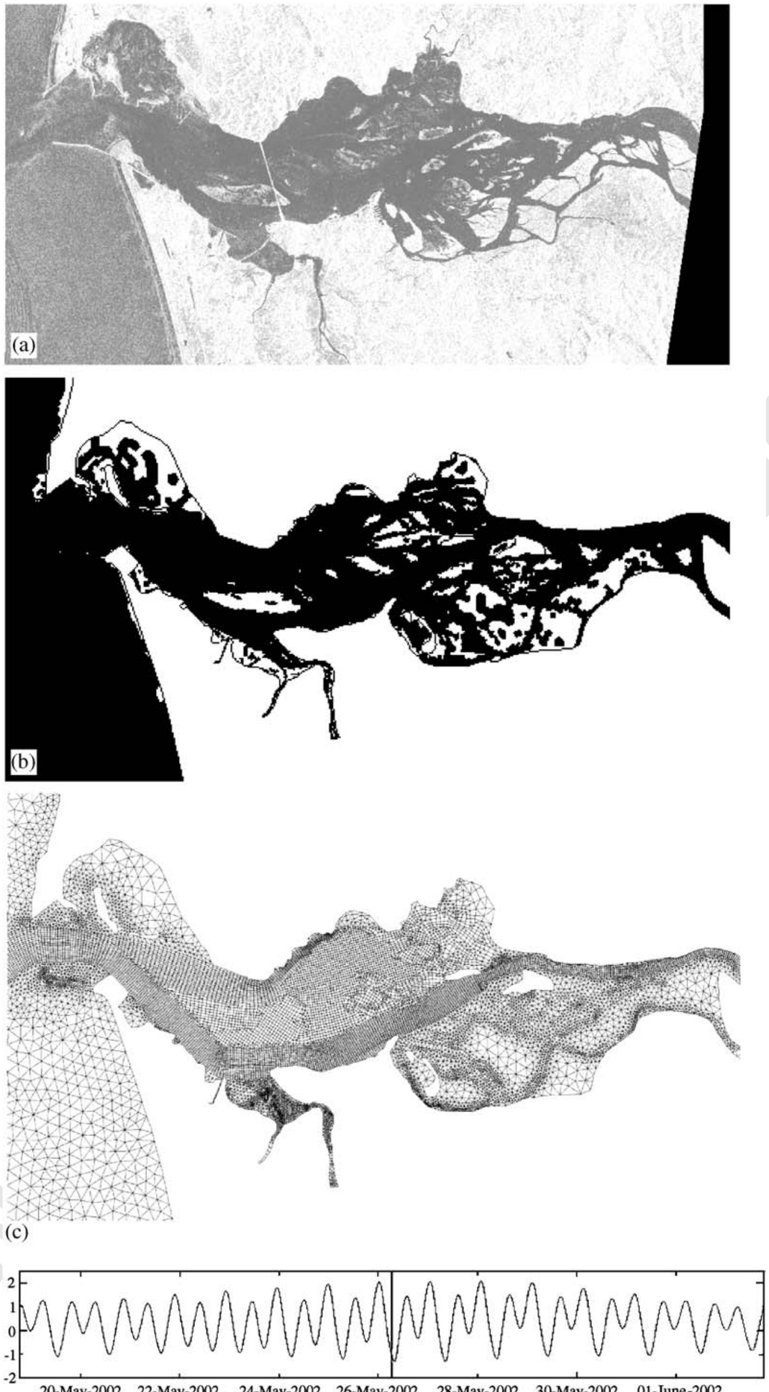

Fig. 15. Wetting and drying in the Columbia River estuary. (a) SAR image, for 05/26/2002 at 06:25 am PST. (b) Baseline simulation for 05/26/2002 at 06:30 am PST. (c) Numerical grid, showing island configuration. (d) Water levels, from observations at Tongue Point.

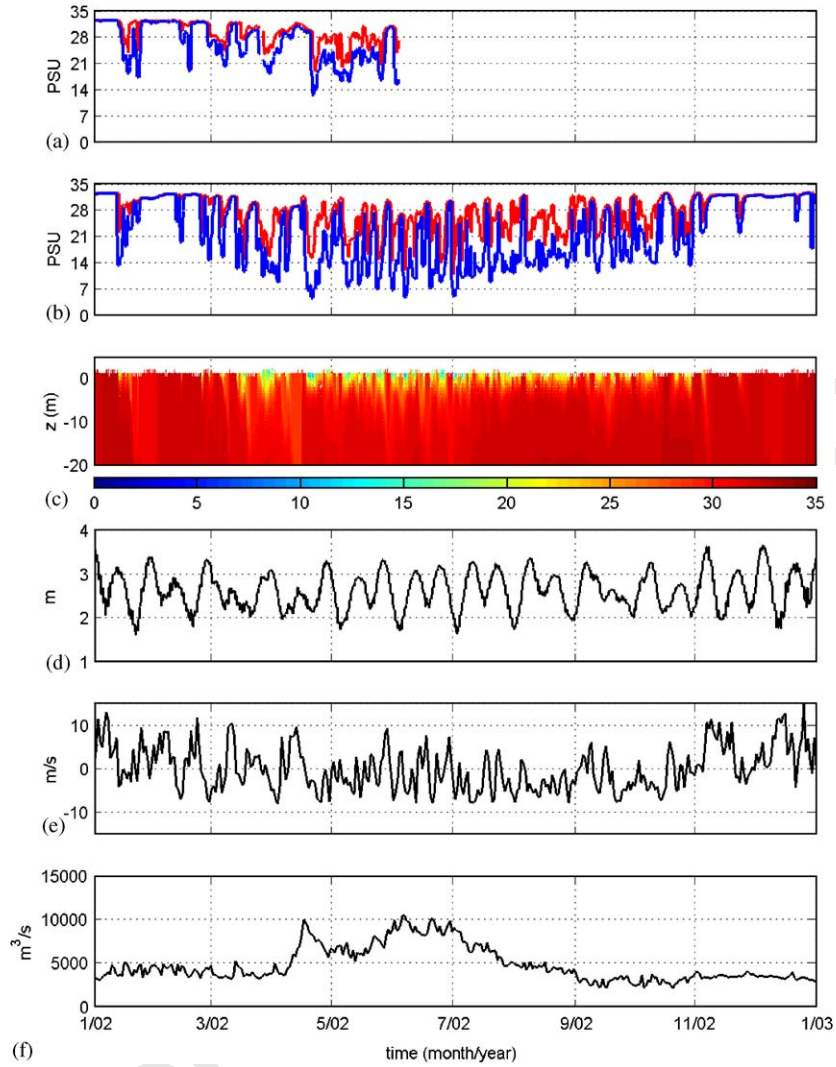

Fig. 16. (a) Observed daily maximum (red) and minimum (blue) salinity at the CORIE station *ogi01*, from a sensor located 1 m below the water surface. (b) Daily maximum (red) and daily minimum (blue) salinity at the surface from DB11. (c) Vertical structure of salinity at ogi01, top 30 m from baseline simulations. (d) Daily tidal range from observations at Tongue Point. (e) N–S component of daily-averaged wind speed from observations at the NOAA buoy 46029. (f) Daily-averaged river discharge measured at Bonneville Dam. Time is denoted by MM/YY.

volume in the estuary behaves qualitatively as expected, responding to both the seasonal variation of river discharges and to spring-neap cycles. Unlike earlier CORIE databases, there are no discontinuities among simulation ensembles in DB11, suggesting that dynamic equilibrium has been reached within each ensemble. The lack of discontinuities validates our strategy of temporal parallelization and suggests that the "response time" of the system is on the order of one to two months. Other sensitivity runs revealed that the more realistic turbulence closure scheme of *k-kl* and the nudging to the NCOM results in the ocean are responsible for the quick convergence of flow fields (not shown here).

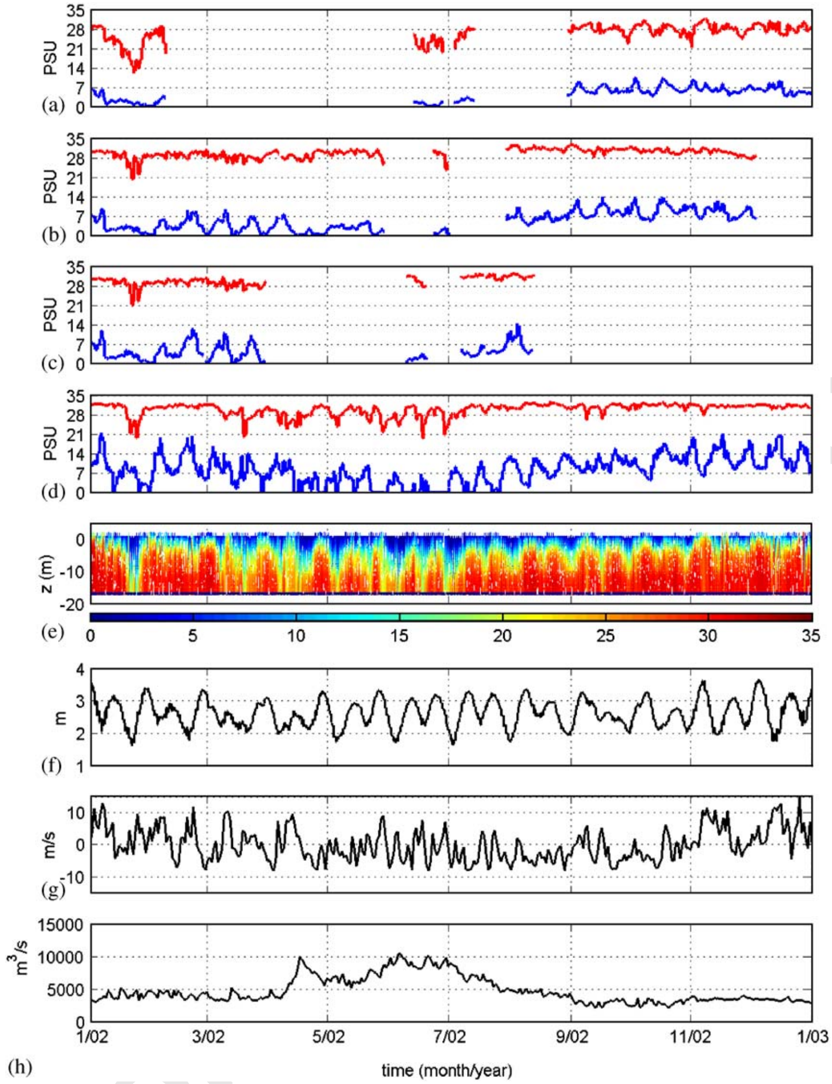

Fig. 17. (a–c) Observed daily maximum (red) and daily minimum (blue) salinity at the CORIE station *red*26 from sensors located at 3.3, 7.5 and 9.0 m below MSL, respectively. (d) Daily maximum (red) and daily minimum (blue) salinity at *red*26, bottom layer, from DB11. (e) Vertical structure of salinity at *red*26 from baseline simulations. (f) Daily tidal range from observations at Tongue Point. (g) N–S component of daily-averaged wind speed from observations at the NOAA 46029 buoy. (h) Daily-averaged river discharge measured at Bonneville Dam. Time is denoted by MM/YY.

Besides fixed stations, scientific cruises are also very useful in gauging the model performance by covering a large area. A comprehensive survey was conducted in May–July 2004, which generated a wealth of observational data. Shown in Figs. 20 and 21 are some preliminary data-model (from CORIE daily forecasts) comparisons: the good qualitative agreement between observed and simulated plume in Fig. 21 shows how dynamic the plume is to the forcing within several days, while Fig. 20 suggests that the model qualitatively captures some key characteristics of the plume, although the modeled plume tends to be fresher than the observed one, especially near the surface.

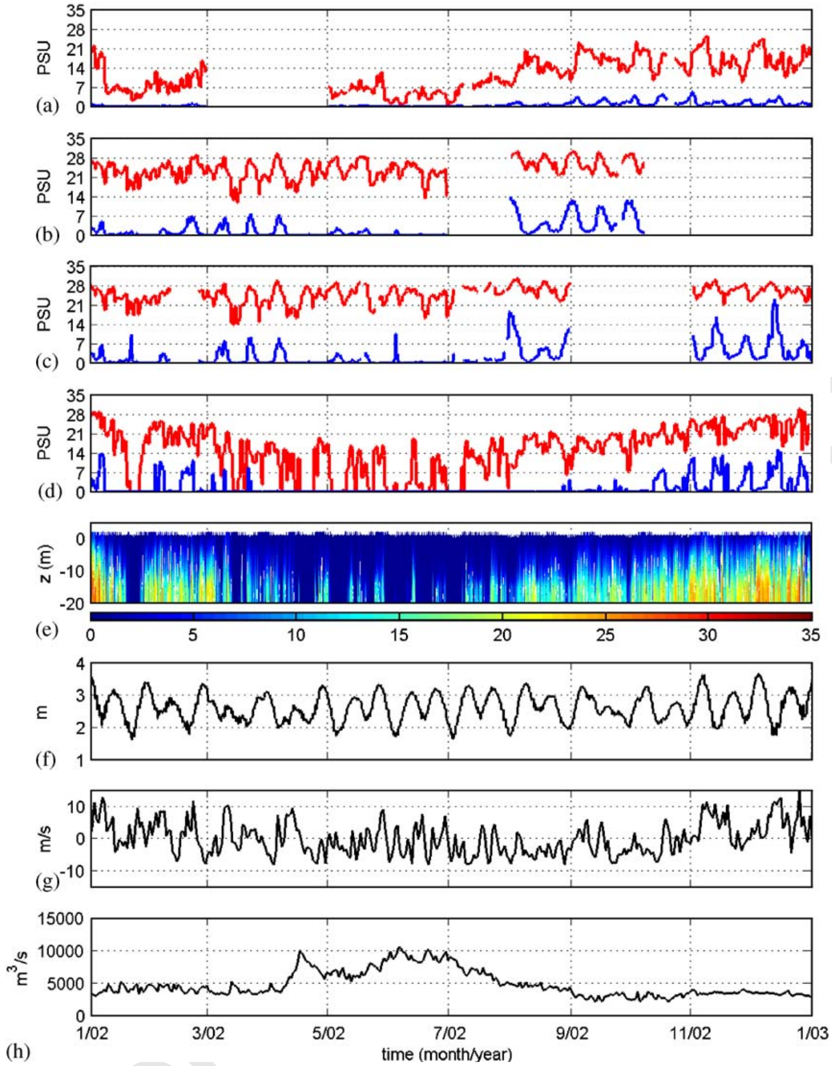

Fig. 18. (a–c) Observed daily maximum (red) and daily minimum (blue) salinity at the CORIE station *am*169 at sensors located at 2.6 m, 11.3 m, and 14.3 m below MSL, respectively. (d) Daily maximum (red) and daily minimum (blue) salinity at *am*169, bottom layer, from DB11. (e) Vertical structure of salinity at *am*169 from baseline simulations. (f) Daily tidal range from observations at Tongue Point. (g) N–S component of daily-averaged wind speed from observations at the NOAA buoy 46029. (h) Daily-averaged river discharge measured at Bonneville Dam. Time is denoted by MM/YY.

A detailed report on the May–July 2004 surveys will be published elsewhere.

3.2. Sensitivity to modeling choices

To explore the sensitivity of the results to modeling choices, we present in this section selected results from various databases and calibration runs as defined in Table 5.

3.2.1. Parameterization of surface stresses

Figure 22 motivated our preference for a particular parameterization of surface stresses (Zeng et al., 1998). This figure shows the week-averaged, root-mean-square errors of low-pass

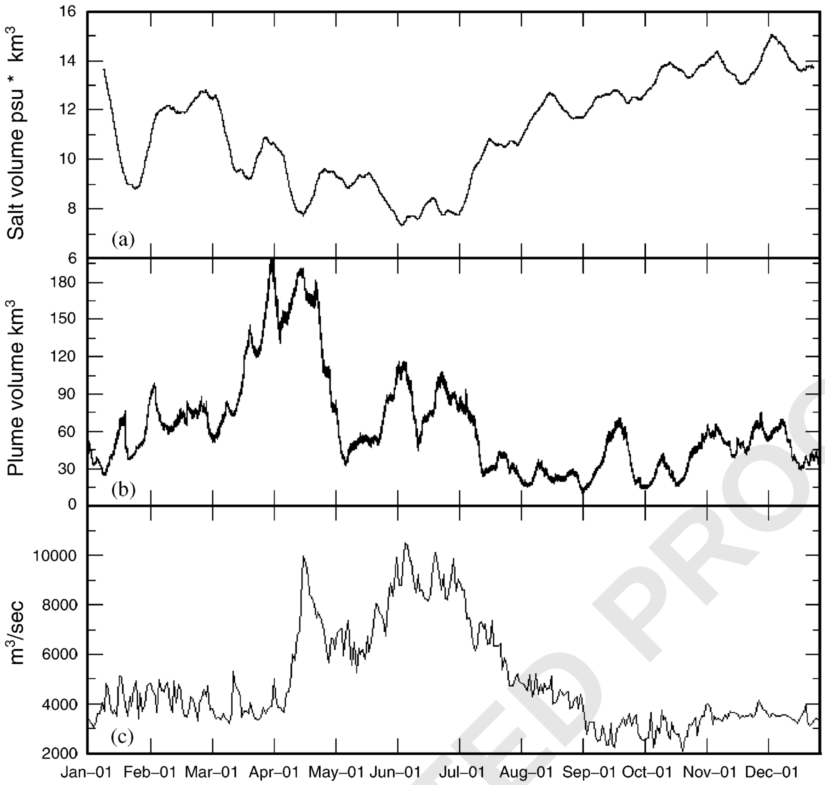

Fig. 19. Integral salt balance metrics computed from DB11. (a) Volume of salt inside the estuary. (b) Plume volume based on the 30psu contour as defined for plume extent. Note that there is no visible sharp discontinuities across ensembles. (c) Daily-averaged river discharge measured at Bonneville dam.

water levels at Tongue Point, contrasted against the x-component (i.e., approximately, the E–W component) of the Ekman transport in the vicinity of the Columbia River. The x-component of the Ekman transport is computed from external forcings and ELCIRC results as (following Cushman-Roisin, 1994):

$$E_k^x = \int_0^T \mathrm{d}t \int_L U(x,y)\,\mathrm{d}s \quad (\text{in m}^3),$$

$$U(x,y) = \int_{-\infty}^0 u(x,y,z)\,\mathrm{d}z = \frac{\tau_y(x,y)}{\rho_0 f} \quad (\text{in m}^2/\text{s}), \qquad (6)$$

where L bounds a rectangle centered at the mouth of the estuary, $T = 7$ days, u is the x-component of the water velocity, τ_y is the y-component of the wind stress, and ρ_0 and f are respectively a reference density and the Coriolis factor.

DB04 and DB05 were built with an early version of ELCIRC (version 4.01, rather than 5.01 used in most recent runs). Like DB06, they were initialized from a Levitus condition and used a zero-equation parameterization of vertical mixing (Pacanowski and Philander, 1981; hereafter, "P&P"), although other set-up details differ from DB06. Most importantly, DB05 is the first hindcast database to use the approach of Zeng et al. (1998) to parameterize surface stresses, while DB04 uses one of the empirical relationships of Pond and Pickard (1998).

DB04 responds to downwelling events early and late in the year with the type of large root mean square errors that were characteristic of early

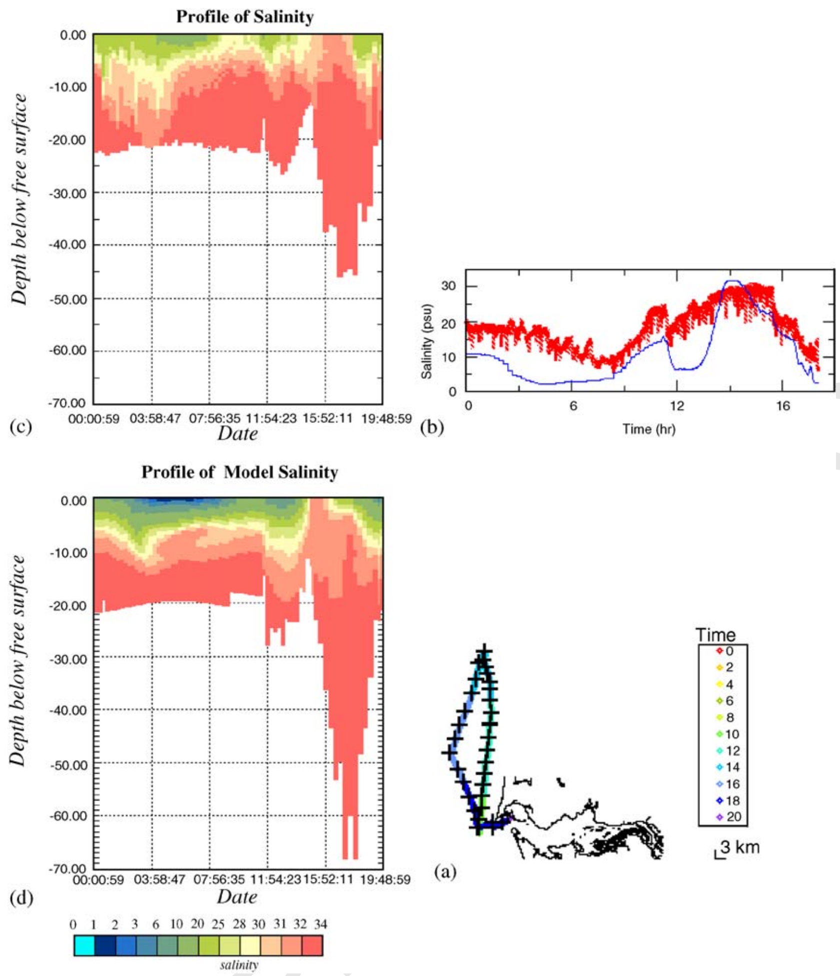

Fig. 20. Comparison of model results to data for an offshore cruise conducted on July 15, 2004. Thermosalinigraph (TSG) data were collected along the entire path (a), and conductivity-salinity-depth (CTD) casts were performed at multiple locations (marked by +). Model and observed data were referenced relative to the free surface. (b) Model data (DB11) from 1 m below the free surface (blue) compared to TSG data (red). (c) Salinity isolines constructed from CTD cast data (location varies over time). (d) Salinity isolines from DB11 along cruise path.

databases and calibration runs, all of which used Pond and Pickard (1998). In DB05, 06, and 11, this type of errors is greatly attenuated relative to DB04. None of the substantial modifications introduced after DB05 (in code formulation, external forcings, or simulation set-up) significantly affects the response of errors to downwelling conditions, thus confirming surface stress parameterization as the transformative element in improving in-estuary responses to coastal winds during downwelling.

The remaining errors in water levels during downwelling regimes are currently being investigated. The prevailing hypothesis is that errors derive predominantly from the difficulty of external forecasts to represent the intensity and the phase of strong winter frontal systems.

3.2.2. Salinity in the estuary and the plume

The transport of salt and heat is very sensitive to vertical mixing. While early databases and calibration runs used P&P, mainly due to its efficiency,

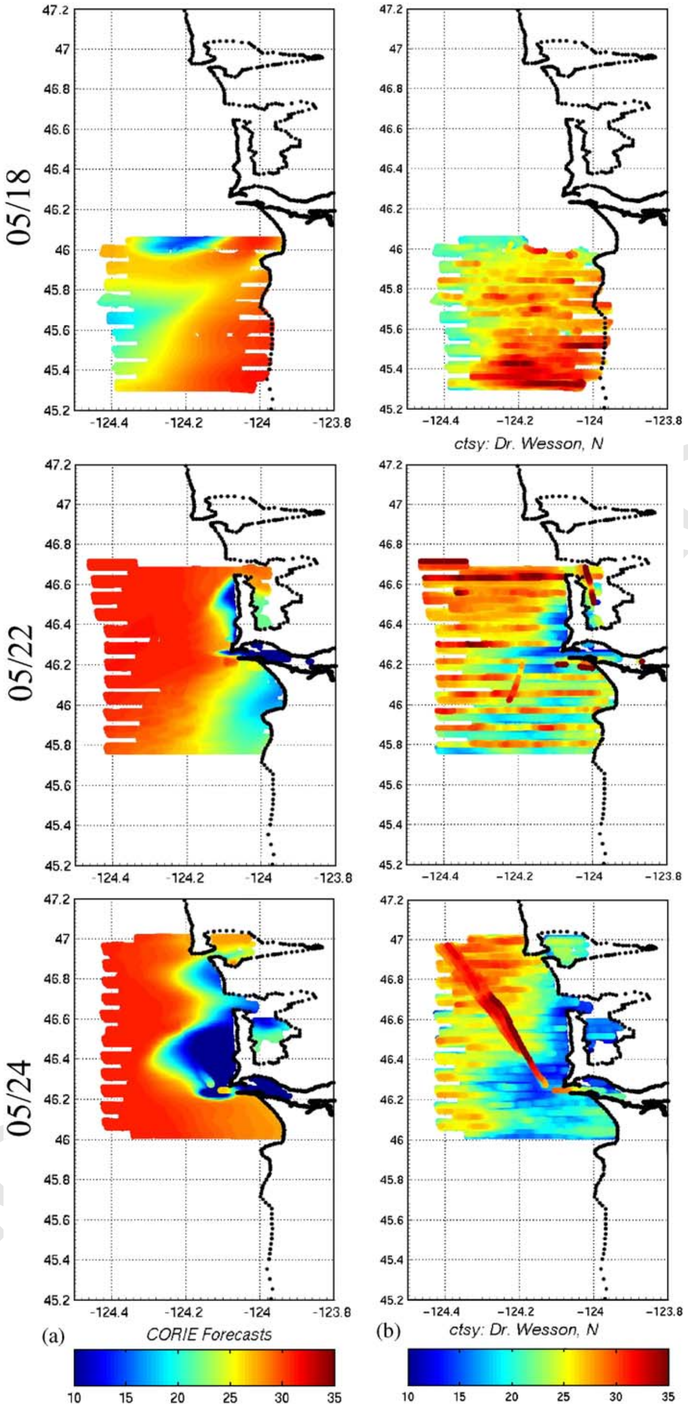

Fig. 21. Comparison of plume profiles for 3 days in May 2004, between (a) model and (b) observation from an airborne survey (courtesy of Dr. Wesson).

Table 5
Summary of runs

	ELCIRC version	Ocean initial conditions	Nudging for ocean S,T	Wind stress formulation	Turbulence closure scheme	Diffusivity limits in the ocean (for *k-kl* only) (m^2/s)	Diffusivity limits in the estuary (for *kl* only)
DB04	4.01	Levitus	No	Pond and Pickard (1998)	Pacanowski and Philander (P&P) (1981)	N/A	N/A
DB05	4.01	Levitus	No	Zeng et al. (1998)	P&P	N/A	N/A
DB06	5.01	Levitus	No	Zeng et al. (1998)	P&P	N/A	N/A
DB10	5.01	NCOM	Yes	Zeng et al. (1998)	*k-kl*	$\upsilon\max = 10$, $\upsilon\min = 10^{-6}$	$\upsilon\max = 10^{-3}$, $\upsilon\min = 10^{-6}$
DB11[a]	5.01	NCOM	Yes	Zeng et al. (1998)	*k-kl*	$\upsilon\max = 10$, $\upsilon\min = 10^{-6}$	$\upsilon\max = 10^{-3}$, $\upsilon\min = 10^{-6}$
C88a	5.01	NCOM	Yes	Zeng et al. (1998)	P&P	$\upsilon\max = 10$, $\upsilon\min = 10^{-6}$	$\upsilon\max = 10^{-3}$, $\upsilon\min = 10^{-6}$
C100a	5.01	$S = 32$psu, $T = 15\,^{\circ}C$	Yes	Zeng et al. (1998)	*k-kl*	$\upsilon\max = 10$, $\upsilon\min = 10^{-4}$	$\upsilon\max = 10^{-2}$, $\upsilon\min = 10^{-6}$
C100b	5.01	S = 35psu, $T = 15\,^{\circ}C$	Yes	Zeng et al. (1998)	*k-kl*	$\upsilon\max = 10$, $\upsilon\min = 10^{-4}$	$\upsilon\max = 10^{-2}$, $\upsilon\min = 10^{-6}$
C100c	5.01	S = 35psu, $T = 15\,^{\circ}C$	Yes	Zeng et al. (1998)	*k-kl*	$\upsilon\max = 10$, $\upsilon\min = 10^{-4}$	$\upsilon\max = 0.0005$, $\upsilon\min = 10^{-6}$
C100e	5.01	S = 35psu, $T = 15\,^{\circ}C$	Yes	Zeng et al. (1998)	*k-kl*	$\upsilon\max = 10$, $\upsilon\min = 10^{-3}$	$\upsilon\max = 10^{-2}$, $\upsilon\min = 10^{-6}$

[a]The main differences between *DB*10 *and DB*11 are that the latter includes the Strait of Geogia and the Fraser River, and uses more recent bathymetric information.

this zeroth order closure did not give satisfactory results in either the plume or the estuary. To demonstrate this, results from DB10 (which uses *k-kl*) and C88a (which uses P&P) (cf. Table 5) are compared; the only difference between them is the turbulence closure scheme used. The results of C88a are very different from DB10, in terms of plume shape and extent (Fig. 23), and salinity-time series inside the estuary (Fig. 24). The overly fresh, large, and non-responsive plume shown in Fig. 23b is typical of all runs using P&P closure.

While DB11 uses *k-kl*, *it* still under-predicts the extent of salt intrusion in the estuary. Hence, further test runs were done to improve the results. Of all choices of model parameters, we were particularly interested in two: the ‘‘background’’ ocean salinity, and the mixing limits inside and outside the estuary. Studying the sensitivity of the simulations to the first parameter was aimed at understanding the impact of underpredicted NCOM salinities in the continental shelf region. Tests focused on the second parameter were designed to understand the sensitivity of the simulations to detailed choices within the *k-kl* closure scheme. To simplify the task, we opted for a non-stratified ocean of constant S, T. All sensitivity runs (C100a-e) were cold-started from week 27 of 2004 and covered 3 consecutive weeks. While details of the runs are in Table 5, we summarize here their major differences:

1. C100b: Base run, with *k-kl* closure, the minimum diffusivity in the ocean being $10^{-4}\,m^2/s$, the maximum diffusivity in the estuary being $10^{-2}\,m^2/s$, and an ocean salinity of 35psu;
2. C100a: C100b with an ocean salinity of 32psu;
3. C100c: C100b with the maximum diffusivity in the estuary being $0.0005\,m^2/s$;
4. C100e: C100b with the minimum diffusivity in the ocean being $10^{-3}\,m^2/s$.

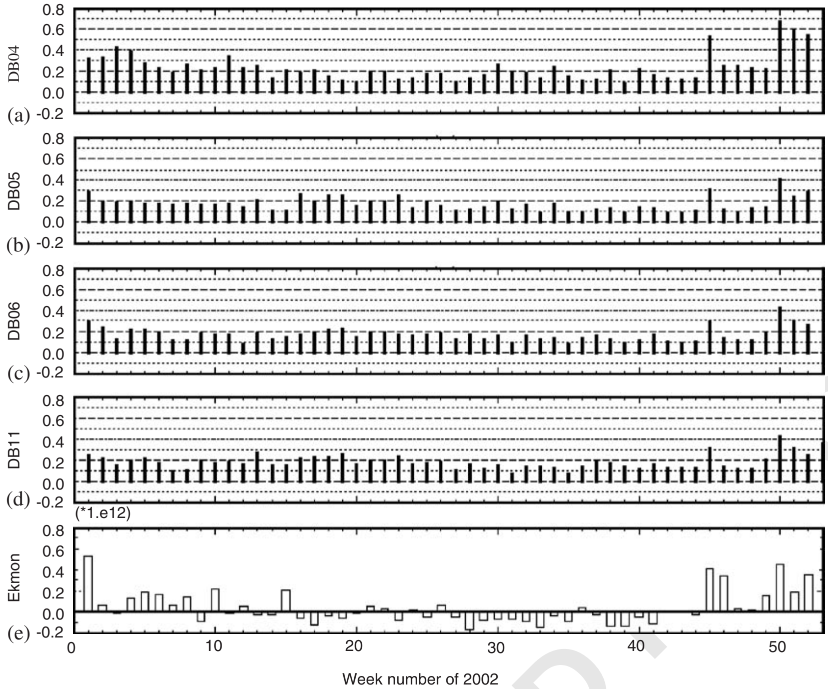

Fig. 22. RMS errors (computed over 1-week intervals) in water levels at Tongue point. (a) Errors in DB04. (b) Errors in DB05. (c) Errors in DB06. (d) Errors in DB11. (e) Ekman transport. Time is in weeks.

Comparisons were made in week 29 for the bottom salinity at the station *am*169 (Fig. 25), as well as the instantaneous intrusion length (from the mouth of the estuary) in the south channel, using 5psu as the cut-off value (Fig. 26). C100c, with a larger ocean salinity to start with and smaller maximum diffusivity in the estuary, provides the best results in all regards, and C100a, with a smaller ocean salinity, provides the worst results. This finding confirms that the ocean supply of salt is important for the salinity intrusion in the estuary. C100e predicts a deeper intrusion but a lower bottom salinity than C100b, indicating that ocean "ambient" mixing also influences the estuary. Larger ambient mixing in the ocean would entrain more salt water but mix it more effectively, thus being consistent with both reduced bottom salinity and stronger salt intrusion. Results suggest an under-prediction of ocean mixing in typical CORIE simulations, which might relate to under-representation of wind stress, or to the neglect of global-scale ocean circulation.

Note that even the best results (C100c) in the above experiment show underpredicted salinity at upstream stations like *am*169. The same trend is generally true for experiments, not reported here, involving moderate refinements of horizontal and vertical grids inside the estuary, sensitivity to bottom-drag coefficients, and updated bathymetry according to more recent surveys. This persistent trend suggests that ELCIRC might be approaching a natural limit in its ability to represent salt propagation without data assimilation.

4. Final considerations

CORIE offers an early example of the inclusion of sustained multi-scale modeling in ocean observatories. Through systematic experimentation, we have made substantial progress towards a physically based description of the baroclinic

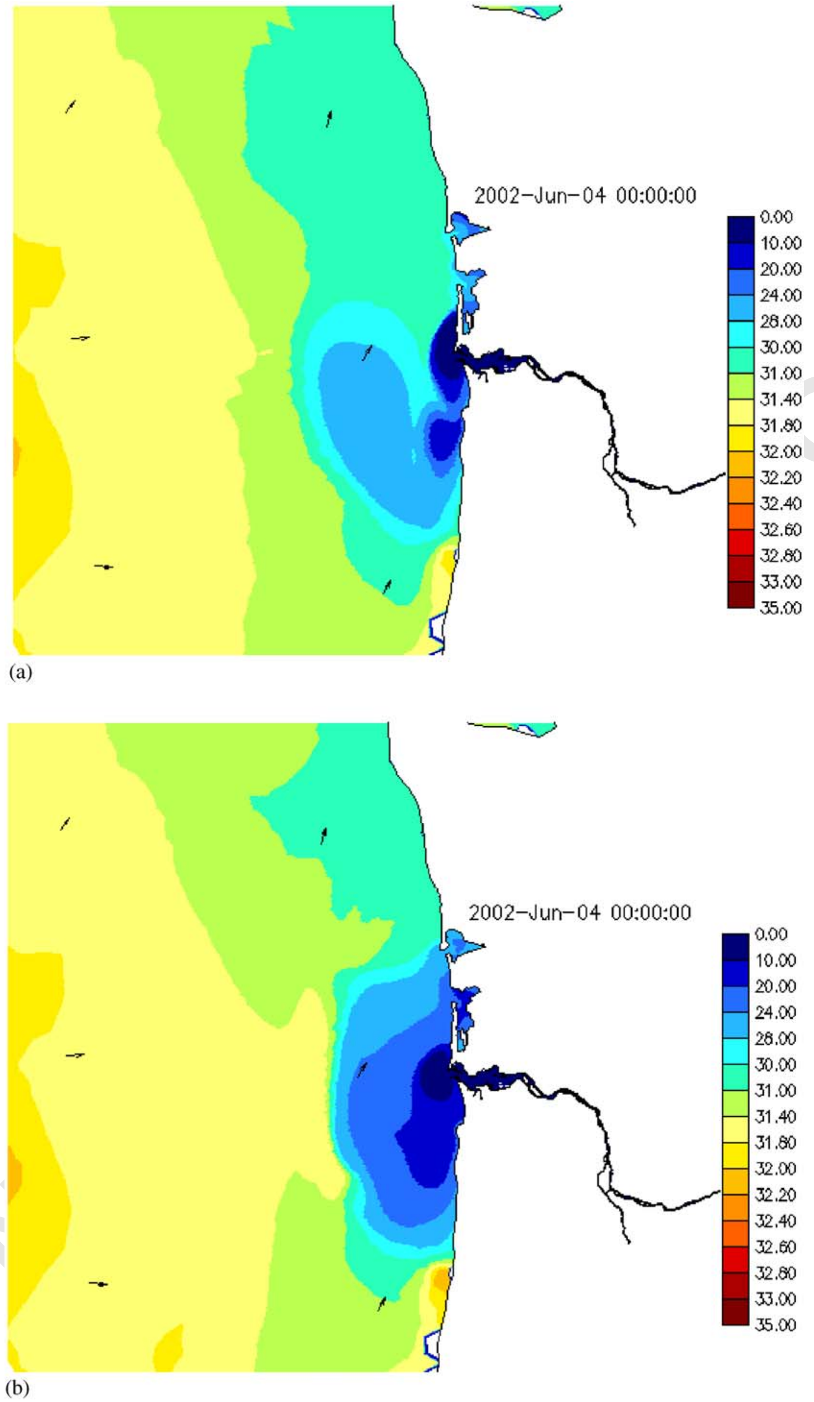

Fig. 23. Comparison of surface plume at the end of week 22 of 2002 between (a) DB10 and (b) C88a.

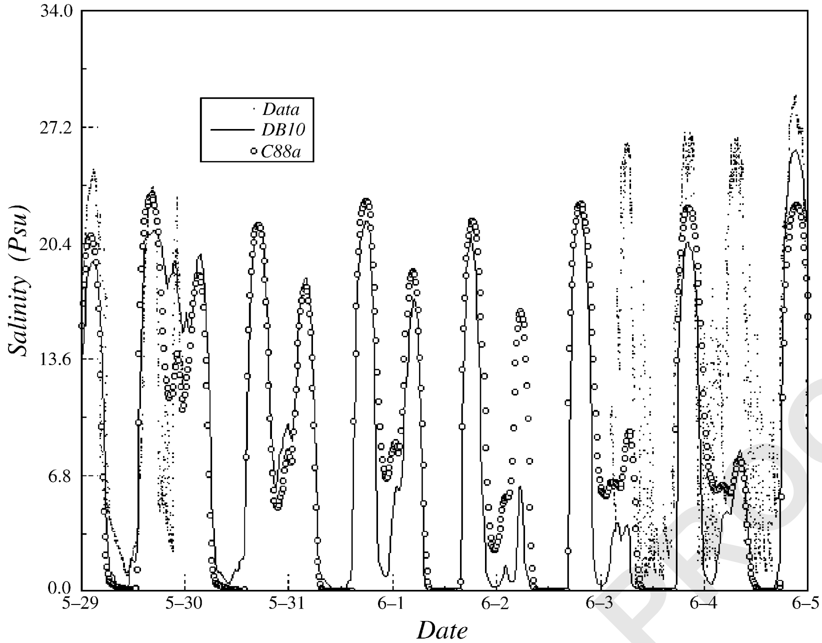

Fig. 24. Comparison of bottom salinity at *tansy* in week 22 of 2002. Note that there is a gap in data.

circulation of the Columbia River estuary and plume.

ELCIRC has been an integral part of that progress. Indeed, the introduction of ELCIRC into the CORIE modeling system in 2001 has been transformative of our ability to conduct a very large number of meaningful, long-term 3D baroclinic simulations. Together with extensive long-term observations, these simulations are providing new insights into the Columbia River circulation.

While we will further develop the theme elsewhere, the modeling work reported here already shows how responsive the Columbia River is to continental shelf processes—thus opening the doors, for instance, to understanding the impact of climatic cycles on the estuary and plume, such as El Niño-Southern Oscillation and Pacific Decadal Oscillation.

From our perspective, two challenges stand in the critical path of CORIE as an effective modeling infrastructure for the Columbia River system. One challenge relates to the computational performance of ELCIRC. Even with the efficiency of its serial version, our ultimate goal of building multiple-decade simulation databases will require the parallelization of ELCIRC, an on-going process. The availability of a parallel ELCIRC, coupled with the 40 CPUs available in the CORIE computer cluster, is expected to significantly change the short-term ability of the CORIE modeling system to generate multi-year hindcast databases.

The other challenge—which we have partially addressed in this paper—relates to an improved description of salt dynamics in the Columbia River estuary and plume. We have already shown that substantial improvements result from the use of a 2.5-equation turbulence closure and the use of ocean conditions derived from the global NCOM model. However, the inability of ELCIRC to resolve the bottom boundary layer and the low-order nature of the ELCIRC algorithm are obstacles that need to be addressed moving forward.

Two options are being considered within CORIE: one involves adding data assimilation to ELCIRC, while the other involves using a newly developed higher-order, terrain-following coordinate model. While the application of the new model has yielded encouraging preliminary results

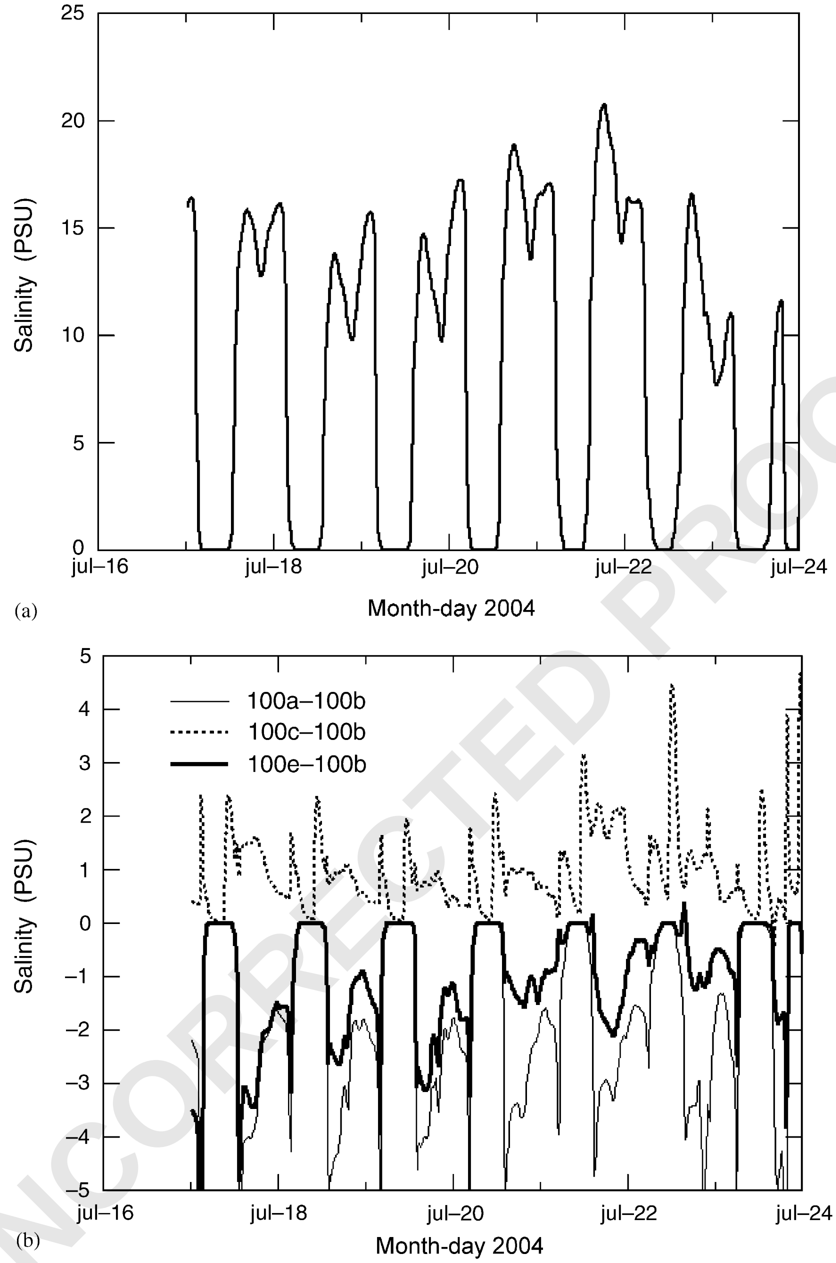

Fig. 25. Comparison of bottom salinity at *am*169 from C100 a–c, and e. (a) C100b. (b) Differences between C100b and others. Note that the true bottom salinity should be much higher for this low discharge period.

for the salinity intrusion in the Columbia River, the eventual path forward will likely be determined by computational considerations. In any case, the robustness, efficiency, and versatility of ELCIRC have already allowed enormous progress in understanding Columbia River circulation, suggesting that ELCIRC is a valuable tool for multi-scale circulation modeling.

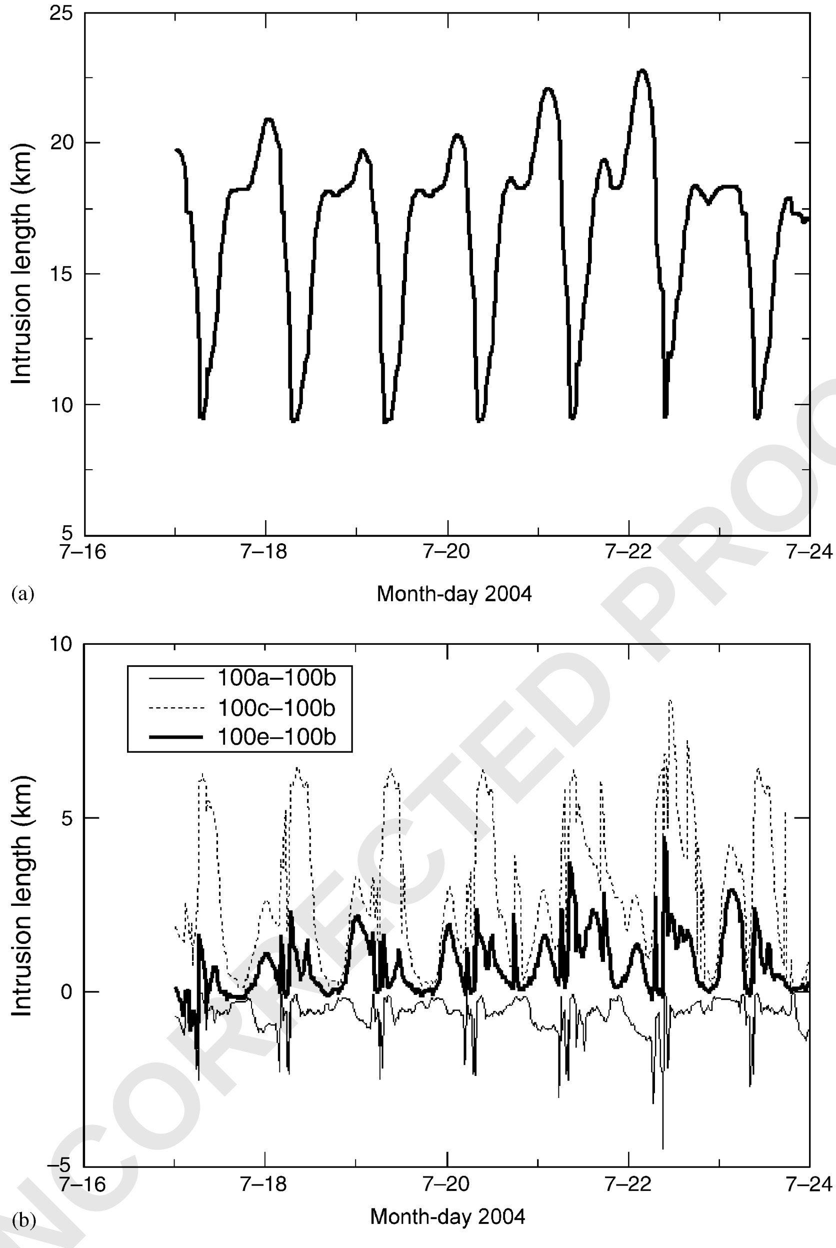

Fig. 26. Comparison of salinity intrusion limits based on 5psu threshold for (a) C100b. (b) Differences between C100b and C100a, c, and e.

5. Appendix. Definition of metrics for grid orthogonality

Following Casulli and Zanolli (1998), a grid is defined as orthogonal if, within each element, a point (“center”, although not necessarily the geometric center) can be identified such that the segment joining the centers of two adjacent elements, and the side shared by the two elements, have a non-empty intersection and are perpendicular to each other.

The indices defined in this section are an attempt to provide a practical, quantitative metric with which to evaluate the extent to which hybrid grids meet the orthogonality requirement. For triangles, we define the index of orthogonality as

$$\vartheta_3 = \frac{2L_{\min}}{R} \quad (-2 \leqslant \vartheta_3 \leqslant 1), \tag{7}$$

where R is the circum-radius of the triangle, and $L_{\min}$ is the minimum signed distance from the circum-center to the three sides (Fig. 7a). The element is orthogonal if $\vartheta_3 > 0$ (otherwise non-orthogonal) and is equilateral if $\vartheta_3 = 1$.

For quadrangles, we define the index of orthogonality as (Fig. 7c):

$$\vartheta_4 = \frac{R_4}{R}, \quad (0 \leqslant \vartheta_4 < \infty)$$

where R is the circum-radius of the triangle formed by nodes 1–3,[2] and R_4 is the distance from node 4 to the circum-center of nodes 1–3. The element is orthogonal if $\vartheta_4 = 1$. Otherwise, it is non-orthogonal. Note that this index for quadrangles assumes that the circum-center is inside the element, a requirement that first needs to be checked.

6. Uncited references

Bottom et al. (2001); Casulli and Walters (2000); Mellor and Yamada (1982); NCEP (2004); Umlauf and Burchard (2003); USACE (2001).

Acknowledgements

The development and testing of the CORIE modeling system has greatly benefited from the contributions of many colleagues. Drs. Todd Leen, David Maier, Claudio Silva, Wu-chi Feng, Wu-chang Feng, and Juliana Freire have brought the formal rigor of computer science to several aspects of CORIE, from automated quality control, to flow and visualization of information, and to product generation. Within the CORIE team, we are particularly grateful to Cole McCandlish, Guangzhi Liu, and Phil Pearson, for the development of several of the standard CORIE products, and to Jon Graves, for support in data collection. We are also grateful to Dr. Edmundo Casillas, of NOAA's Northwest Fisheries Science Center, for providing a driving application and partially facilitating the funded development of CORIE. The CORIE modeling system has been developed and maintained through a combination of projects funded by NOAA and the Bonneville Power Administration (NA17FE1486, NA17FE1026, NA87FE0405), the US Fish and Wildlife Service (133101J104), the Office of Naval Research (N00014-00-1-0301, N00014-99-1-0051), and the National Science Foundation (ACI-0121475). Appreciation is extended to Sergio deRada, Charley Barron, and Lucy Smedstad for help in providing the global NCOM fields. Support for one of the authors (Kindle) was provided through the Naval Research Laboratory 6.1 project "Coupled Physical and Bio-optical modeling in the Coastal Zone", under program element 61153N sponsored by the Office of Naval Research. Dr. Todd Sanders provided the SAR image in Fig. 15a under NOAA NESDIS Grant NA16EC2450. Dr. Joel Wesson of Naval Research Laboratory provided the airborne survey data in Fig. 21b.

Any statements, opinions, findings, conclusions or recommendations expressed in this paper are those of the authors and do not necessarily reflect the views or policies of the federal sponsors, and no official endorsement should be inferred.

[2] In a stricter sense than used in this paper, indices should arguably be computed using all combinations of three consecutive nodes within the quadrangle.

References

Baptista, A.M., 2002. Environmental observation and forecasting systems. In: Meyers, R.A. (Ed.), Encyclopedia of Physical Science and Technology, vol. 5. Academic Press, New York, p. 16.

Baptista, A.M., Wilkin, M., Pearson, P., Turner, P., McCandlish, C., Barrett, P., Das, S., Sommerfield, W., Qi, M., Nangia, N., Jay, D., Long, D., Pu, C., Hunt, J., Yang, Z., Myers, E., Darland, J., Farrenkopf, A., 1998. Towards a multi-purpose forecast system for the Columbia River

Estuary. Ocean Community Conference '98. Baltimore, Maryland.

Baptista, A.M., Wilkin, M., Pearson, P., Turner, C., McCandlish, C., Barrett, P., 1999. Coastal and estuarine forecast systems: a multi-purpose infrastructure for the Columbia River. Earth System Monthly (NOAA) 9(3).

Baptista, A.M., Zhang, Y.-L., Chawla, A., Zulauf, M.A., Seaton, C., Myer, E.P., Kindle, J., Wilkin, M., Burla, M., Turner, P.J., 2004. CORIE modeling system: status of hindcast simulations as of May 2004. http://www.ccalmr.ogi.edu/CORIE/modeling/elcirc/.

Barnes, C.A., Duxbory, A.C., Morse, B.A., 1972. Circulation and selected properties of the Columbia River effluent at sea. In: Alverson, D.L., Pruter, A.T. (Eds.), The Columbia River Estuary and Adjacent Ocean Regions: Bioenvironmental Studies. University of Washington Press, Seattle, WA, pp. 41–80.

Blumberg, A.F., Mellor, G.L., 1987. A description of a three-dimensional coastal ocean circulation model. In: Heaps, N. (Ed.), Three-Dimensional Coastal Ocean Models. AGU, Washington, DC, pp. 1–16.

Bottom, D.L., Simenstad, C.A., Baptista, A.M., Jay, D.A., Burke, J., Jones, K.K., Casillas, E., Schiewe, M.H., 2001. Salmon at River's End: The Role of the Estuary in the Decline and Recovery of Columbia River Salmon. National Marine Fisheries Service.

Casulli, V., Cattani, E., 1994. Stability, accuracy and efficiency of a semi-implicit method for 3D shallow water flow. Computers & Mathematics with Applications 27 (27), 99–112.

Casulli, V., Walters, R.A., 2000. An unstructured grid, three-dimensional model based on the shallow water equations. International Journal for Numerical Methods in Fluids 32, 331–348.

Casulli, V., Zanolli, P., 1998. A three-dimensional semi-implicit algorithm for environmental flows on unstructured grids. Conference on Numerical Methods for Fluid Dynamics, vol. VI, Institute for Computational Fluid Dynamics.

CCALMR (1996–2004). CORIE Observation and Forecasting System. (http://www.ccalmr.ogi.edu/CORIE), Center for Coastal and Land-Margin Research, Oregon Health & Science University.

Chawla, A., Baptista, A.M., Jay, D.A., Wilkin, M. Long term variability of circulation in the Columbia River estuary. Journal of Geophysical Research, in preparation.

Clark, H.L., Isern, A., 2003. The OOI and the IOOS—can they be differentiated? an NSF perspective. Oceanography 16, 20–21.

CRETM, 1990–2000. Columbia River Estuarine Turbidity Maxima. (http://depts.washington.edu/cretmweb/CRETM.html), LMER/CRETM Team. 2001.

Cushman-Roisin, B., 1994. Introduction to Geophysical Fluid Dynamics. Prentice-Hall, Englewood Cliffs, NJ.

Egbert, G.D., Bennett, A.F., Foreman, M.G.G., 1994. TOPEX/POSEIDON Tides estimated using a global inverse model. Journal of Geophysical Research 99 (24), 821–824, 852.

Foreman, M.G.G., 1977. Manual for Tidal Heights Analysis and Prediction, vol. 58. Institute of Ocean Sciences, Patricia Bay, Sidney, BC.

Fox, D.N., Teague, W.J., Barron, C.N., Carnes, M.R., Lee, C.M., 2002. The modular ocean data assimilation system (MODAS). Journal of Atmospheric and Oceanic Technology 19, 240–252.

Frolov, S., Baptista, A.M., Leen, T.K., 2004. Calibration of spatio-temporal-varying bottom drag in an estuary with multiple dynamical and error regimes. Eos Trans. AGU 84(52), Portland, OR, Ocean Sci. Meet. Suppl., Abstract OS51C-09.

Garcia-Berdeal, I., Hickey, B.M., Kawase, M., 2002. Influence of wind stress and ambient flow on a high discharge river plume. Journal of Geophysical Research 107 (C9), 3130.

Glenn, S.M., Boicourt, W., Parker, B., Dickey, T.D., 2000. Operational observation networks for ports, a large estuary and an open shelf. Oceanography 13, 12–23.

Grimes, C.B., Kingsford, M.J., 1996. How do riverine plumes of different sizes influence fish larvae: do they enhance recruitment? Marine & Freshwater Research 47, 191–208.

Hamilton, P., 1990. Modelling salinity and circulation for the Columbia River estuary. Progress in Oceanography 25, 113–156.

Hickey, B.M., Pietrafesa, L.J., Jay, D.A., Boicourt, W.C., 1998. The Columbia River plume study: subtidal variability in the velocity and salinity fields. Journal of Geophysical Research 103 (C5), 10,339–13,368.

Jay, D.A., Smith, J.D., 1990. Residual circulation in shallow estuaries, II. Weakly stratified and partially mixed, narrow estuaries. Journal of Geophysical Research 95 (C1), 733–748.

Levitus, S., 1982. Climatological Atlas of the World Ocean, vol. 173. Princeton, NJ, NOAA/ERL GFDL.

LMER Coordinating Committee (W. Boyton, J. T. H., D.A. Jay, M. Kemp, J. Kremer, C. Simenstad, S.V. Smith, I. Valiela) (1992). Understanding changes in coastal environments: the land-margin ecosystems research program. EOS 73, 481–485.

Martin, D.L., 2003. The national oceanographic partnership program, ocean US, and real movement towards an integrated and sustained ocean observing system. Oceanography 16, 13–19.

Martin, P.J., 2000. Description of the Navy Coastal Ocean Model Version 1.0. Naval Research Laboratory.

Mellor, G.L., Yamada, T., 1982. Development of a turbulence closure model for geophysical fluid problems. Review of Geophysics 20, 851–875.

Myers, E.P., Baptista, A.M., 2001. Inversion for tides in the Eastern North Pacific Ocean. Advances in Water Resources 24 (5), 505–519.

NCEP, 2004. Operational ETA: Output Grid Coverage (http://wwwt.emc.ncep.noaa.gov/mmb/etagrids/). National Centers for Environmental Prediction.

Pacanowski, R.C., Philander, S.G.H., 1981. Parameterization of vertical mixing in numerical models of tropical oceans. Journal of Physical Oceanography 11, 1443–1451.

Parker, B.B., 1997. Development of model based regional nowcasting/forecasting systems. In: Spaulding, M.L., Blumberg, A.F. (Eds.), Estuarine and Coastal Modeling. ASCE, New York, pp. 355–373.
Pond, S., Pickard, G.L., 1998. Introductory Dynamical Oceanography. Butterworth, Heinmann, London.
Reid, R.O., 1990. Waterlevel changes. In: Herbich, J. (Ed.), Handbook of Coastal and Ocean Engineering. Gulf Publishing, Houston, TX.
Rhodes, R.C., Hurlburt, H.E., Wallcraft, A.J., Barron, C.N., Martin, P.J., Smedstad, O.M., Cross, S., Metzger, J.E., Shriver, J., Kara, A., Ko, D.S., 2001. Navy Real-Time Global Modeling Systems. Oceanography 15 (1), 29–43.
Rosmond, T.E., Teixeira, J., Peng, M., Hogan, T.F., Pauley, R., 2002. Navy operational global atmospheric prediction system (NOGAPS): Forcing for Ocean Models. Oceanography 15 (1), 99–108.
Steere, D., Baptista, A.M., McNamee, D., Pu, C., Walpole, J., 2000. Research Challenges in Environmental Observation and Forecasting Systems. Mobicom 2000. ACM Press, Boston, MA.
Umlauf, L., Burchard, H., 2003. A generic length-scale equation for geophysical turbulence models. Journal of Marine Research 6 (12), 235–265.
USACE, 2001. Biological assessment—Columbia River Channel improvements project. An Internal Report to the National Marine Fisheries Service and US Fish and Wildlife Service US. Army Corps of Engineers, Portland District.
USCOP, 2004. Preliminary Report of the US Commission on Ocean Policy—Governors' Draft (http://www.oceancommission.gov/documents/prelimreport/welcome.html), US Commission on Ocean Policy.
Zeng, X., Zhao, M., Dickinson, R.E., 1998. Intercomparison of bulk aerodynamic algorithms for the computation of sea surface fluxes using TOGA COARE and TAO data. Journal of Climate 11, 2628–2644.
Zhang, Y., Baptista, A.M., 2004. Benchmarking a new open-source 3D circulation model (ELCIRC). Computational Methods in Water Resources. Chapel Hill, NC.
Zhang, Y., Baptista, A.M., Myers, E., 2004. A cross-scale model for 3D baroclinic circulation in estuary-plume-shelf systems: I. formulation and skill assessment. Continental Shelf Research, in press.